Heterogeneous & Homogeneous & Bio- & Nano-
CHEMCATCHEM
CATALYSIS

Accepted Article

Title: Recent Developments in Heterogeneous Catalysts Modelling for CO2 Conversion to Chemicals

Authors: Natalia Podrojkova, Victor Sans Sangorrin, Andrej Orinak, and Renata Orinakova

To be cited as: *ChemCatChem* 10.1002/cctc.201901879

Link to VoR: http://dx.doi.org/10.1002/cctc.201901879

A Journal of
ChemPubSoc Europe

WILEY-VCH

www.chemcatchem.org

10.1002/cctc.201901879

Recent Developments in Heterogeneous Catalysts Modelling for CO_2 Conversion to Chemicals

N. Podrojková[a], V. Sans[b], A. Oriňak*[a], R. Oriňaková[a]

[a]*Department of Physical Chemistry, Faculty of Science, P.J. Šafárik University, Moyzesova 11, 041 54 Košice, Slovakia*

[b]*Institute of Advanced Materials (INAM), Universitat Jaume I, Avda. Sos Baynat s/n, 12006, Castellón de la Plana, Spain*

Abstract: Density functional theory (DFT) of the CO_2 behaviour on the catalyst surface provides valuable insights about the C=O bond activation, information about adsorption and dissociation of CO_2, understanding the elementary steps involved in the mechanism of the CO_2 hydrogenation reaction. Nowadays, DFT computational studies for the catalytic hydrogenation of CO_2 are becoming very popular. Therefore, this article is focused on a comprehensive review of the DFT studies in thermocatalytic hydrogenation of CO_2 at the gas-surface interface and discusses three aspects: 1) processes taking place on the surfaces and facets of transition metal heterogeneous catalysts, 2) adsorption of CO_2 on surfaces of different transition metals; 3) current understanding of reaction mechanisms taking place on the catalytic surface for the production of different compounds. A detailed schematic overview of the possible CO_2 hydrogenation mechanisms and DFT simulations presented here will enhance the current understanding of the CO_2 catalytic hydrogenation.

Acronyms and nomenclature

Latin letters:

ΔH	Enthalpy
ΔG	Gibbs free energy

Geek letters:

Γ	Surface energy

Acronyms:

BET	Brunauer–Emmett–Teller
BEEF-vdW	Bayesian error estimation with van der Waals correlation functional
CI-NEB	Climbing image nudged elastic band
DFT	Density functional theory
DFT-PW91	Plane-wave density functional theory
DNP	Double-numerical quality basis set with polarization function
FCD	Full charge density
FTS	Fischer–Tropsch synthesis
GAM	Gradient approximation for molecules functionals
GGA	Generalized gradient approximation
HSE06	Hybrid exchange–correlation functional
LDA	Local-density approximation
M06-L	Minnesota 2006 local functional
MAEAM	Modified embedded-atom method
mBEEF-vdW	meta-generalized Bayesian error estimation with van der Waals correlation functional
ML	Metal-ligand
MN15-L	Minnesota nonseparable 2015 local functional
MS2	“made simple” metaGGA functional
RPA	Random phase approximation

RWGS	Reverse Water-Gas-Shift
PAW	Projector augmented wave
PBE	Perdew-Burke-Ernzerhof
PBEsol	Revised Perdew-Burke-Ernzerhof GGA
PW91	Perdew and Wang's 1991 GGA
PW-DFT	Plane-wave density functional theory
PW-GGA	Plane-wave generalized gradient approximation
PWSCF	Plane-Wave Self-Consistent Field
RPBE	revised PBE GGA
SCAN	Strongly Constrained and Appropriately Normed
SP-DFT	Spin-polarized density functional theory
vdW-DF	Rutgers-Chalmers van der Waals Density Functional
WGS	Water-Gas-Shift

Material Related Symbols:

25Ni-3Mn-Al_2O_3	Aluminium oxide loaded with 25 wt% of Ni and 3 wt% of Mn as a promoter
40Ni-Nb_2O_5-700	Niobium pentoxide loaded with 40 wt% of Ni and calcinated at 700°C
β-Mo_2C	Orthorhombic molybdenum carbide crystal structure
$Ce_{1.1}Cu_1$	Cerium-copper catalyst with mole ratio of 1.1:1 prepared by reduction of cerium-copper oxide
CNTs	Carbon nanotubes
FeCO(S-η_1-C)	Isomer of Fe(111)/CO intermediate with CO coordinated to Fe through C on shallow site
$FeCO_2$-(S-μ_3-C,O,O´)	Isomer of Fe(111)/CO_2 intermediate with CO_2 coordinated to Fe through C and O on shallow site
FeX(B-μ_3-X)	Isomer of Fe(111)/C and Fe(111)/O intermediates with C and O atoms coordinated to Fe through X = C and O on bridge site
FeX(T,S-μ_2-X)	Isomer of Fe(111)/C and Fe(111)/O intermediates with C and O atoms coordinated to Fe through X = C and O on top and shallow site
Mo_2C	Molybdenium Carbide
M-CeO_2	Hexagonal Molybdenium Carbide
Pd_3Cu_6	Three Cu atoms on the topmost layer of 3×3 Cu(111) periodic surface slab replaced by Pd atoms, describes the formation of Pd dimers over Cu(111)
Pd_6Cu_3	Six Cu atoms on the topmost layer of 3×3 Cu(111) periodic surface slab replaced by Pd atoms, describes the formation of Pd trimers
Rh_3Cu_6	Three Cu atoms on the topmost layer of 3×3 Cu(111) periodic surface slab replaced by Rh atoms

1. Introduction

The increasing average temperature of the Earth's atmosphere is a global environmental problem which continues to grow as a consequence of a constantly rising carbon dioxide (CO_2) concentration in the atmosphere. Upper scenarios for CO_2 emissions show the rise of CO_2 concentration up to 936-1200 ppm by 2100 with global temperature increase by 3 – 5.5°C.[1]

Under the conservative scenarios atmospheric CO_2 levels are forecasted to remain below 450 – 550 ppm with mean global temperature 1.5°C and an increase of global mean sea level between 0.26 to 0.77 m.[1,2] Hence, it is imperative to reduce the emissions of CO_2. Developing efficient methods to employ CO_2 as an abundant C1 building block to produce chemicals, materials, fuels or carbohydrates is a very attractive approach.

10.1002/cctc.201901879

Natália Podrojková received her MSc. degree from Pavol Jozef Šafárik University in Košice in 2018. In 2017 she joined the IHRS BioSoft Guest Student Programme 2017, where she worked at the University of Cologne under the supervision of Prof. Annette Schmidt. Currently, she is a Ph.D. student under the guidance of Prof. Oriňak at the Department of Physical Chemistry, Pavol Jozef Šafárik University in Košice. Her current research focuses on synthesis, characterisation of ZnO/Cu nanocatalysts and their use in CO_2 hydrogenation.

Victor Sans graduated in Chemical Engineering at the University Jaume I followed by a MSc and a PhD in Sustainable Chemistry. After he took a post-doctoral appointment at the University of Bath and later Warwick under the supervision of Prof. Alexei Lapkin. Since 2011 he worked in the Cronin group as a PDRA and since 2013 as a Research Fellow in the same group. In 2014 he was appointed Assistant Professor and promoted to Associate Professor in 2018 at the University of Nottingham. Currently, he is a CIDEGENT Fellow and group leader at the Institute of Advanced Materials (INAM) at the Universitat Jaume I. His research interest include reactor engineering, 3D-printing, advanced materials, sustainable chemical processing and process autoation.

Andrej Oriňak studied chemistry at the Pavol Jozef Šafárik University in Košice and completed his PhD in 1995 at the Slovak University of Technology in Bratislava. After finishing his habilitation at Slovak University of Technology in Bratislava in 2001, he was in 2013 appointed professor for Analytical Chemistry at the Slovak University of Technology in Bratislava. Currently, he is working at Department of Physical Chemistry at the Pavol Jozef Šafárik University in Košice. His research interests cover a broad spectrum of different field of chromatography, preparation of functional surfaces for physical applications and developing nanocatalysts for energy conversion, hydrogen production among others.

Renáta Oriňaková studied chemistry at the University of Pavol Jozef Šafárik in Košice and completed her PhD in 1997 at the Comenius University in Bratislava. She is now a professor for Physical Chemistry, vice-dean for international affairs and research at faculty of Science and head of the Department of Physical Chemistry at the Pavol Jozef Šafárik University and she is president of scientific group for Physical Chemistry and Electrochemistry of Slovak Chemical Society in Košice. Her research interests focus on electrochemical deposition of functional nanostructured materials for analytical applications, sensors, electrocatalysis, biomedicine, and integration into miniaturised systems as well with production of biodegradable materials for orthopaedic applications.

In the case of chemical CO_2 utilization, CO_2 is typically converted by thermochemical processes such as homogeneous[3,4] and heterogeneous hydrogenation;[5,6] and by biochemical[7], electrochemical,[5,8–10] photochemical[11] and photoelectrochemical reduction processes.[12,13] The use of specific catalysts is key to overcome high activation energy barriers, to extend the electrode life and stability or to capture solar radiations that generate excitons (e^- + hole) for CO_2 reduction.[14,15] For the CO_2 conversion processes heterogeneous catalysts are preferred and widely used in the industries. They exhibit high catalytic activity, robustness, high efficiency in the recovery and recycling with the possibility of simple product separation, which can be economically advantageous in industrial CO_2 conversion. They also provide significant durability and stability in handling and reactor design.

The publication activity for catalytic CO_2 conversion by hydrogenation, electrochemical and photochemical reduction was examined by a bibliometric analysis which was performed using the SCI-expanded search platform and the search results are shown in Figure 1. Currently, the most examined area is electrochemical way of CO_2 conversion. Electrochemical CO_2 reduction has received a great deal of attention recently, but the low solubility of CO_2 in aqueous solution has been a major obstacle which leads to mass transport limitation.[16,17] The use of a gas diffusion electrode has enabled the direct use of gaseous CO_2 for electrochemical conversion because the electrochemical conversion process does not require H_2 as a reactant.[17] The attention towards photochemical reduction started increasing from 2012. Because of its similarity to photosynthesis, the process typically suffers from low productivity and poor stability.[17]

Figure 1 Timeline for the number of articles published on CO_2 hydrogenation, electrochemical and photochemical reduction using the SCI-Expanded search platform.

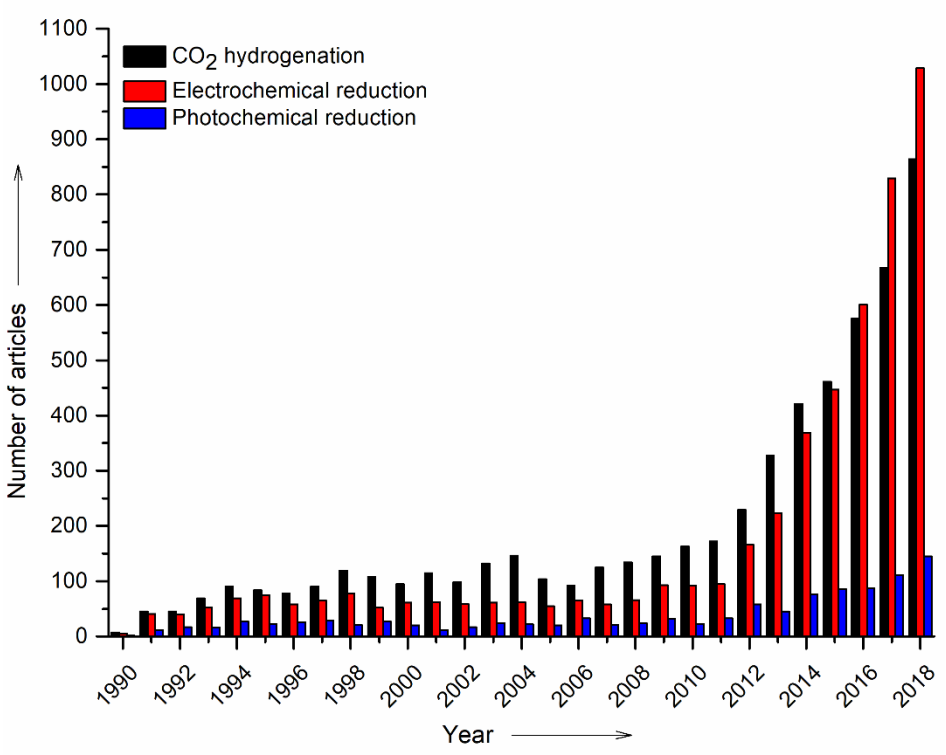

The most widely used method of CO_2 conversion is catalytic hydrogenation. Several articles about current experimental research of the CO_2 hydrogenation summarize the development of the most recent catalysts with proposed mechanisms.[5,18–21] The majority of the literature is focused on methanol synthesis and mechanism of methanol formation on mainly used and most debated ZnO/Cu catalytic surface[22–26] which makes it more accessible to find information about reaction pathways for methanol production. Information about reaction intermediates and reaction pathways on various catalytic surfaces for preparation of other chemicals is not easily obtainable. Therefore, this review summarizes and systematizes mechanisms for CO_2 hydrogenation using catalysts based on different type of transition metals.

The use of quantum mechanics simulations for understanding the CO_2 hydrogenation process is effective in finding new intermediates, searching for new catalysts, and identifying reaction pathways.[27] The DFT simulation of CO_2 behaviour on the surface of the catalysts can provide invaluable insights about the C=O bond activation, help to understand the evolution adsorbed species on the surface of the catalyst, information about rate-determining step, and overall insight into reaction mechanism which can speed up and diminish the system cost significantly and contribute to obtain a better understanding of the catalyst role. DFT is helpful to understand the nature of chemical reaction deeply from the molecular level, study the reaction including every primitive step, then find the pathway of chemical reaction, and eventually find out the key points affecting the reaction rate.[28] In the case of literature that is oriented towards DFT simulations of the CO_2 hydrogenation on catalytic surface there is one review[27] that solely summarizes theoretical results and one review that is more oriented towards mechanisms of solid–gas interface thermocatalytic CO_2 reduction. Since more and more studies use different DFT methods for calculating reaction mechanisms the findings vary with each article. Therefore, recent findings need to be aligned and compared with experimental results in order to obtain information about the effect of different catalyst more easily or indicate which way the experimental and theoretical research should continue in the future. Hence, the discussion is aimed at results of computational studies of elementary processes between reactants and catalysts, their structures, reaction pathways with focus on systematization as well the reliability of DFT calculations.

The article is divided into two chapters. The first chapter deals with the CO_2 hydrogenation and various catalysts used for the preparation of different products. Possible reaction pathways are described with schematic presentation, and current challenges and possible solutions are introduced. The second chapter is focused on recent progress on catalyst's surface modelling. Beginning of the chapter is dedicated to the surface and adsorption energies calculated by DFT and other theoretical methods with discussion dedicated to comparison of DFT calculations using multiple functionals. Second half of the chapter describes all transition metal surfaces that were examined with DFT method for CO_2 hydrogenation. Results are divided depending on which product of the hydrogenation was supposed to be prepared. CO_2 adsorption on metal surfaces together with adsorption, surface energies and proposed mechanisms that include the effect of different catalyst type are all discussed.

2. Current understanding of CO_2 catalytic hydrogenation

In CO_2, carbon is in its highest oxidation state which makes the compound thermodynamically very stable with C=O bond dissociation energy (750 kJ mol^{-1}) much higher than the C-C (336 kJ mol^{-1}), C-O (327 kJ mol^{-1}) or C-H (441 kJ mol^{-1}).[13] To break such a stable bond, higher temperatures during conversion processes are needed where an increase in temperature facilitates CO_2 activation. However, with a high temperature, the whole process of conversion is energetically very demanding and can result in higher selectivity towards undesirable products. By introducing another substance with higher Gibbs energy as co-reactant, such as hydrogen, the conversion will become thermodynamically easier.[29] To resolve these problems several processes of CO_2 conversion such as thermochemical, electrochemical and photochemical reduction with the use of catalysts have been developed. An appropriate catalyst will decrease the temperature of the process and improve the selectivity.

The CO_2 hydrogenation to hydrocarbons can be seen as a modified FTS with CO_2 as a reactant instead of carbon monoxide (CO).[30] Some of the main products of CO_2 hydrogenation are methanol (CH_3OH), methane (CH_4), formic acid (HCOOH) and hydrocarbon fuels (represented by −CH2-) depending on the type of the catalyst (Table 1) and reaction conditions. CO and water (H_2O) are considered by-products. The endothermic RWGS is widely used as the intermediate step in combination with exothermic reactions that lead to the formation of methanol and hydrocarbon fuels. The production of methanol and hydrocarbon fuels by CO_2 hydrogenation is regarded as the most viable way of reducing CO_2 emissions in the atmosphere significantly.[31,32] Light olefins such as ethylene and propylene are produced worldwide in amounts exceeding 200 million tons per year and are very important building blocks in chemical industry.[33]

Many catalysts have been explored to achieve selective control towards industrially widely demanded products. As shown in table 1, each hydrogenation reaction prefers a different metal-based catalyst type which improves selectivity towards the specific compounds. For RWGS, the most commonly used catalysts are based on Cu-, Pt-, Rh-, Fe-, Ce-, while catalysts based on Cu- together with Cu/ZnO-based catalysts enhance the formation of methanol. For CO_2 methanation Ru-, Fe-, Ni-, Co-, Mo-based catalysts are the most effective and the formation of formic acid is reached with Ru-, Rh-, Ir-, Pd-based catalysts, although various studies have been reported employing Ni[34,35] or Cu[36,37] based catalysts.

Table 1. Main reactions occurring during CO_2 hydrogenation

Hydrogenation reactions	ΔH [kJ.mol^{-1}]	ΔG [kJ.mol^{-1}]	Most commonly used catalysts	Ref.
$CO_2 + H_2 \rightleftharpoons CO + H_2O$	41.2	28.6	Cu-, Pt-, Rh-, Fe-, Ce- based catalysts	[27,38]
$CO_2 + 4H_2 \rightleftharpoons CH_4 + 2H_2O(g)$	-164.9	-113.5	Ru-, Fe-, Ni-, Co-, Mo- based catalysts	[39,40]
$CO_2 + 3H_2 \rightleftharpoons CH_3OH + H_2O(l)$	-131.0	-9.0	Cu- and Cu/ZnO-based catalysts, Pd-, based catalysts	[41,42]
$CO_2 + H_2 \rightleftharpoons HCOOH(l)$	-31.2	33.0	Ru-, Rh-, Ir-, Pd- based catalysts	[40]
$nCO_2 + 3nH_2 \rightleftharpoons C_nH_{2n} + 2nH_2O$	-128			[19]

Most of these catalysts are used and examined in combination with support where mostly metal-oxides[43,44], -carbides[44–46], -sulphides[47,48] and -nitrides[49] are used. Metal oxides are frequently used as supports for the dispersion of metals and reduced oxides have a strong tendency to react with CO_2.[44] Metal-carbides due to their bonding between carbon atom and transition metal atom have unique properties such as high melting temperature (> 3300 K), high hardness (> 2000 kg/mm^2) and high tensile strength (> 300 GPa) and show catalytic activity similar to activity of noble metals.[45,46,50] Metal-nitrides are characterized by two different effects: ligand effect and ensemble effect.[51] Ligand effect results in changes in their electronic structure which strengthens adsorption of reactants and products similar to noble metals improving the selectivity of reaction. Ensemble effect decreases the number of available metal sites and results in creating of different adsorption sites.

Several theoretical studies are devoted to examination of CO_2 behaviour on these surfaces.[52–55] However, this is a difficult task. One of the example are transition metal oxides which are difficult to model using DFT with simple local and semi local functionals.[56] LDA and GGA approximations do not account properly for exchange and correlation effects in transition metal oxides and lead to self-interaction errors.[52] A better description of metal oxide surfaces is provided by self-interaction correction (SIC) and GW approximations (GWA) but these methods are computationally very demanding and not appropriate for the large systems that are required to surfaces and clusters simulations. The only method that takes account the on-site Coulombic repulsion among localized d−electrons by incorporating an extra energetic penalty for delocalization and is relatively computationally low costing is DFT+U method. Also, the results obtained by DFT studies greatly vary depending on the used method which leads to diverse conclusions. The use of the right functional is not trivial and is still highly discussed between researchers not only for complicated systems but also for transition metal surfaces. We think that metal-oxides, -carbides, -sulphides and -nitrides require separate review devoted to computational studies of these surfaces and therefore, this review is aimed mainly on the computational studies of transition metal surfaces and their impact on CO_2 hydrogenation.

2.1. Carbon monoxide formation

Carbon monoxide formed by RWGS reaction is a feedstock or key intermediate for the production of methanol, hydrocarbon fuels via FTS[57] and a building block for carbonylation reactions.[58,59] The RWGS reaction is endothermic (Table 2) and thermodynamically favoured at high temperatures with pressure-independent chemical equilibrium[60] and direct gas-phase reaction which makes it one of the most promising high-temperature chemical reactions.[61]

2.1.1 Potential reaction mechanisms via RWGS

The literature classifies the reaction mechanism into two categories; the redox mechanism and associative mechanism.[62] In the redox mechanism the oxidation reduction cycle occurring on the catalyst surface is responsible for the reaction.[63] CO_2 is firstly adsorbed on the reduced metal sites or metal oxide sites, and then subsequently reacts with them to form CO. After that the oxidized catalyst is reduced by H_2 and the reduced sites are formed again.[64,65]
The associative mechanism, also known as dissociative[66,67] or formate[6,27,68] mechanism is an adsorption - desorption model where the adsorbed species interact to form an adsorbed intermediate (carbonate, formate, carbonyl, etc.) as a critical step in the RWGS process which then decomposes to form H_2 and a mono-dentate carbonate.[64,69] Prevailingly a bidentate formate reaction intermediate is produced through the CO_2* reaction with dissociated H* by the adsorption of preferably oxygen atoms to the metal surface. Additional hydrogenation leads to the formation of HCOOH which splits into HCO* and O* and subsequently into CO* and H*. For the hydroxyl pathway CO_2 is adsorbed onto the surface with carbon and oxygen atoms followed by hydrogenation. COOH* intermediate is then hydrogenated to form COH* and O* that leads to formation of CO* and H* or may be directly dissociated into CO*and O*. Additional O* and H* intermediates lead to H_2O formation. The associative mechanism is depicted in figure 2.

Table 2. Redox mechanism of CO formation

Redox mechanism
$H_2 + 2^* \rightarrow H^* + H^*$
$CO_2 + * \rightarrow CO_2^*$
$CO_2^* + * \rightarrow CO^* + O^*$
$H^* + O^* \rightarrow OH^* + *$
$H^* + OH^* \rightarrow H_2O^*$
$OH^* + OH^* \rightarrow H_2O^* + O^*$
$H_2O^* \rightarrow H_2O + *$
$CO^* \rightarrow CO + *$

2.1.1 RWGS catalysts and challenges

The RWGS studies of supported metal catalysts consist primarily of Cu[70,71], Pt[72,73], and Rh[74] immobilized on a variety supports.[38] Catalysts that are active in the WGS reaction are also active in the RWGS reaction according to the principle of microscopic reversibility.[27] Cu has been shown to perform RWGS at low temperatures,[75,76] and little or no methane is formed as a side product. But without hydrogen, CO_2 dissociation is highly unfavourable on clean Cu surfaces, which directly translates to the need for high H_2/CO_2 feed ratios to achieve high CO_2 conversions.[38] Therefore, Cu demands a support and is combined with other metals. From the recent studies Zou et al.[77] investigated CeCu composite catalysts with different Ce/Cu mole ratios due to high capability to form oxygen vacancies and reversible reducibility of CeO_2 as support. The $Ce_{1.1}Cu_1$ catalyst demonstrated high stability and the highest CO_2 conversion rate in the RWGS reaction with 100% selectivity towards CO, reaching 1.38 $mmol.g_{cat}^{-1}min^{-1}$ at 400 °C. Efficient and stable Cu-based catalyst was also prepared and examined by Zhang et al.[78] They studied effect of β-Mo_2C transition metal carbide on dispersion, stabilisation of copper nanoparticles and subsequently their activity in RWGS reaction. The strong interaction between Cu and β-Mo_2C effectively promoted the dispersion of supported copper and prevented the aggregation of Cu particles which led to extraordinary activity and stability for

RWGS reaction. Noble metal catalysts, mainly Pt and Rh based supported catalysts, have high activity towards hydrogen dissociation, relatively moderate strength with the adsorption of reaction intermediates and the incompletely filled D-orbital electrons make them easier for the adsorption of reactants with moderate strength, which is further benefiting to form the intermediate "active compound" in RWGS reaction.[62] Besides mentioned catalysts other metal catalysts as active components or as supports are Pd,[79] Ni,[80,81] Co,[82,83] Fe,[84] Fe supported on CNTs[85] and carbide (Mo_2C) catalyst.[86,87]

As a support for different metal catalysts Al_2O_3, CeO_2, TiO_2 and SiO_2 are primarily examined. Ni-Al_2O_3 catalyst was investigated by Wolf et al.[88] They achieved the CO_2 equilibrium conversion of 80% at 900°C and proved the catalyst's stability at 900°C. TIO_2 was investigated in combination with Pt at 200-500°C by Chen et al.[89] Pt-O_v-Ti^{3+} species formed at the interface between Pt and reducible TiO_2 support was identified as the active sites for the formation of CO, while large Pt particles facilitated the hydrogenation of CO to CH_4. Dai et al.[88] studied the RWGS reaction on mesoporous M-CeO_2 catalysts. According to their results, CO_2 RWGS reaction catalytic activities decrease in the order Ni-CeO_2 > Cu-CeO_2 > Co-CeO_2 > Fe-CeO_2 ≈ Mn-CeO_2. Besides, Cu-CeO_2, Fe-CeO_2, and Mn-CeO_2 catalysts maintained 100 % CO selectivity at the temperature 400°C. Pt was investigated in combination with TiO_2 or SiO_2 as a support by different researchers[90,91] where the supports promoted the overall CO_2 conversion, although the impact on the selectivity was rather small. To improve the Pt/TiO_2 catalytic impact on RWGS reaction Lee et al.[92] investigated the effect of CeO_2 addition to a Pt/TiO_2 at temperature range 300-600°C. CeO_2 affected the lattice and pore structure through substitution with TiO_2 and optimized the catalyst activity.

Figure 2 Associative mechanism of CO formation: a) formation of HCOO intermediate, b) formation of COOH intermediate.

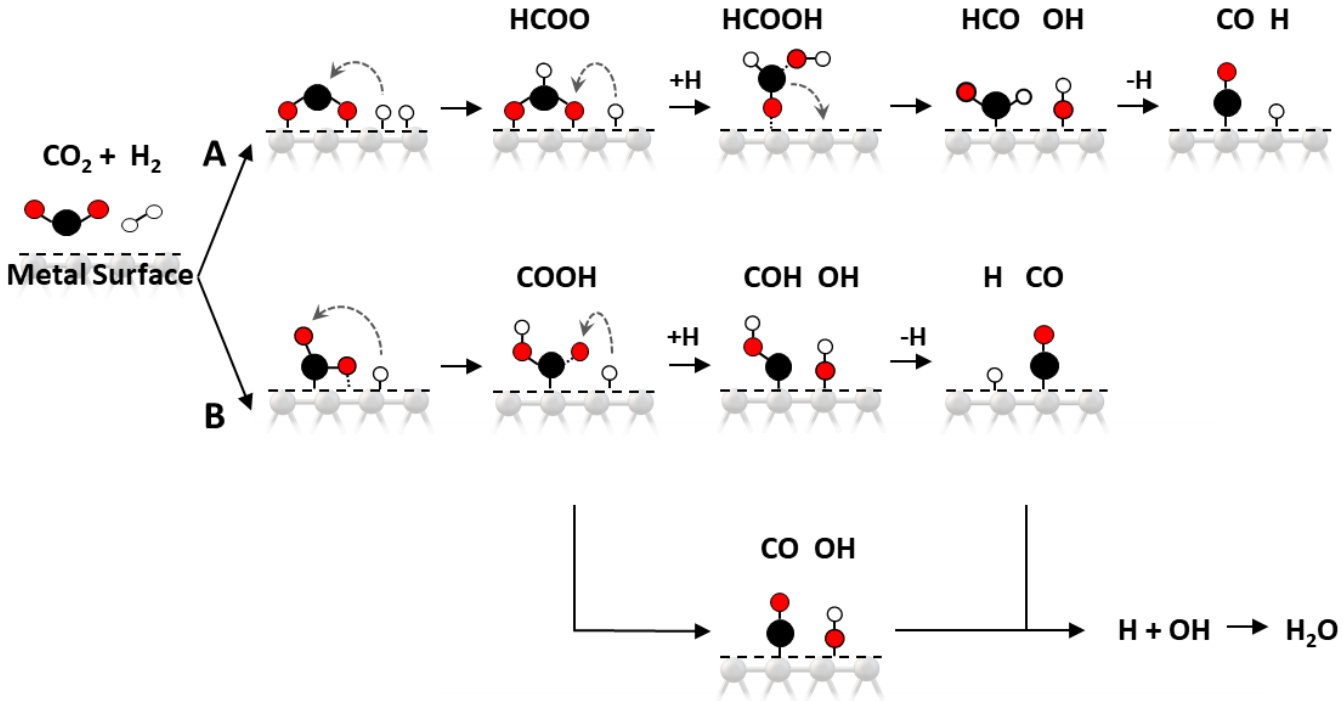

Despite the comprehensive studies conducted to develop high-performance catalysts for the RWGS reaction, a fundamental understanding of the roles of the metal catalysts and their mechanisms during the spontaneous, dynamic, and high-temperature RWGS reaction is lacking.[93] Since the thermodynamics of the RWGS reaction requires high temperatures to reach satisfactory levels of conversion, hence an additional challenge is to improve catalytic activity for the RWGS reaction at lower temperatures maintaining an acceptable CO selectivity.[94]

2.2. Methane synthesis

Due to the increasing demand for mitigating global warming and storing surplus renewable power, the CO_2 methanation or Sabatier reaction is an advantageous way to store renewable energy such as wind and solar power, to transfer biogas effectively to biomethane, and to convert CO_2 to chemical feedstocks and fuels.[19] The CO_2 methanation is exothermic, pressure dependent and is thermodynamically favourable at low temperatures (ΔG^{298K} = –130.8 kJ/mol). However, the reduction of the fully oxidized carbon to methane is an eight-electron process (Eq. 1 and 2) with significant kinetic limitations, which requires a catalyst to achieve acceptable rates and selectivity and makes the process kinetically favourable.[60,95]

2.2.1 Associative and dissociative CO_2 methanation mechanism

The reaction mechanism proposed for CO_2 methanation (figure 3) is divided into two main categories, associative and dissociative mechanism. The first one involves the direct hydrogenation of CO_2 to methane without the formation of CO as an intermediate.[95] The associative adsorption of CO_2 and H_2 adatom H_{ad} is followed by the hydrogenation of the associated species to form methane.[96,97] The other one involves the conversion of CO_2 to CO prior to methanation, and the subsequent reaction follows the same mechanism as CO methanation.[98] CO methanation over supported metal catalysts proceeds via the dissociation of CO on the metal and the hydrogenation of the resultant surface carbonaceous species.[96,99]

Figure 3 Reaction mechanisms possible for the methanation of CO_2: a) associative methanation, b) dissociative methanation, c) CO associative pathway, d) CO dissociative pathway

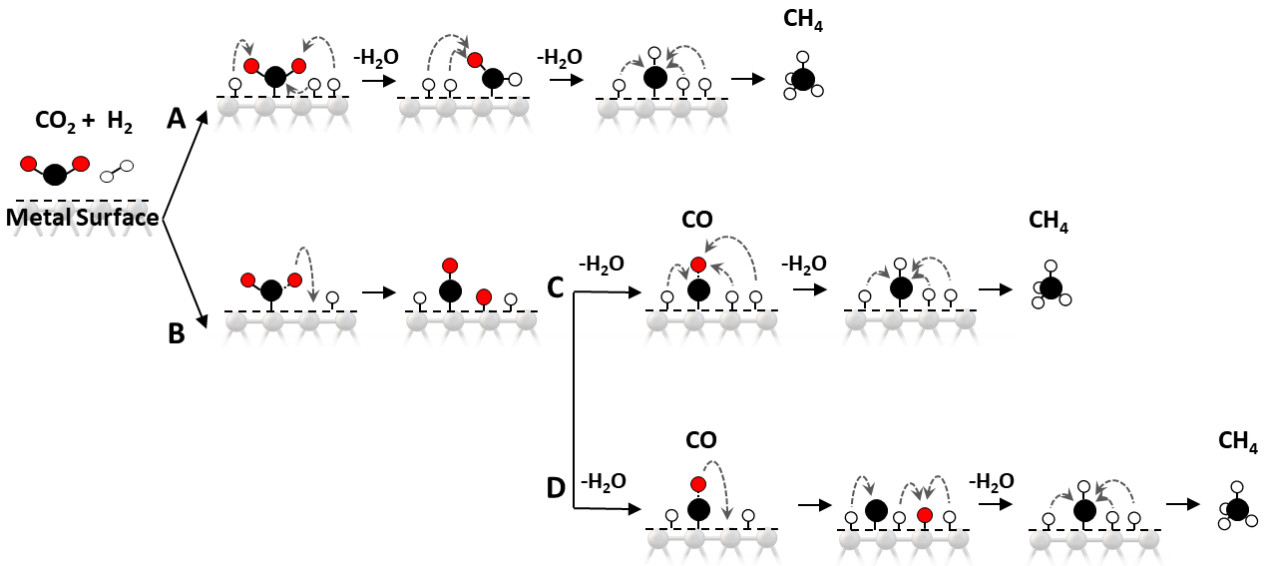

2.2.2 Challenges in catalytic CO_2 methanation

CO_2 methanation can reach 99% CH_4 selectivity through the use of appropriate catalysts, avoiding the subsequent product separation and overcoming the difficulty of dispersed product distribution.[19] The most studied noble and nonnoble metal-based catalysts for CO_2 methanation are Ni,[100–102] Ru,[103–105] Rh,[106,107] Pd,[108,109] Co,[110,111] Fe,[112,113] Cu,[114,115] Pt,[116] Ag[39] and Au[39] catalysts from which the most important role to methanation process has Ru, Fe, Ni, and Co.[39,117] According to the various studies the activity performance and selectivity of different metal-based catalysts decreases in the following

order: Ru > Rh > Ni > Fe > Co > Pt > Pd and Pd > Pt > Ni > Rh > Co > Fe > Ru subsequently.[118] Ni and Ru are reported to have maximum activity and stability.[119] Ni based catalysts are very effective due to the presence of easily transferable electrons in the frontier d orbitals and therefore are the most efficient and active catalytic system together with alumina as a support that may be applied on industrial scale.[120,121] Ru catalysts at 300 °C results in a 96% methane yield while Ni catalysts shows a maximum yield of 80 % at 400 °C.[40] Ru is about 120 times more expensive than Ni and Ni catalysts have a short lifetime, because of carbon deposition which blocks pores and consequently deactivates the catalyst.[39,122] A rational design of Ni-based methanation catalysts with high activity at low temperatures, good redox properties, and better stability at reaction temperatures are still required for industrial applications.[121] Gnanakumar et al.[123] prepared nickel-niobia catalyst 40Ni-Nb_2O_5-700 with CO_2 conversion of 92% and CH_4 selectivity of 99% and catalyst showed stable activity during a continuous test of 50 h. According to their results the strong acid sites seemed to be more favourable for the CO_2 hydrogenation, however they could not find the direct reason for this. Several studies observed promotional role of transition metals on catalytic performance and stability of Ni-Al_2O_3. Daroughegi et al.[124] studied incorporation of Cr, Fe, Mn, Cu and Co into Ni-Al_2O_3. The 25Ni-3Mn-Al_2O_3 catalyst with the highest BET surface area and the lowest crystalline size improved the low temperature activity and selectivity toward methane and passed a stable activity at 350 °C for 10 h in CO_2 methanation reaction. Garbarino et al.[125] observed the effect of Ni/La-Al_2O_3 catalysts on CO_2 methanation. The introduction of lanthanum at low loadings strongly increased the catalytic activity in the 500–630K temperature region, with increase in methane selectivity to ~ 100%. The addition of lanthanum resulted in the formation of basic sites which adsorbed CO_2 more strongly.
From other transition metal catalysts, pure Fe has low activity and selectivity towards methanation and consequently is not active metal in CO_2 methanation.[126] However with the use of a support[127] or in combination with other metals such as Ni[128,129] or Co[130] the activity may increase. Even though Co catalysts are more expensive, they show a similar activity to Ni in CO and CO_2 methanation and also do not require an induction period[39] that is observed with Ni catalysts and necessary to an increase of the Ni particle size.[131]

2.3. Methanol synthesis

Methanol as one of the most valuable chemicals obtainable by CO_2 hydrogenation is not only considered as easily-transport liquid energy storage medium with high energy density, but also served as an essential chemical feedstock with a wide range of utilization ways[132] to produce different chemicals such as formaldehyde, acetic acid, methyl methacrylate, dimethyl terephthalate, methylamines, dimethyl ether, methyl tert-butyl ether, chloromethanes or light olefins.[133]
From a thermodynamic point of view, lower reaction temperature or a higher reaction pressure favours the synthesis of methanol. Indeed, enhanced reaction temperature (e.g., higher than 513 K) facilitates CO_2 activation and subsequent methanol formation. Furthermore, other by-products are formed during the hydrogenation of CO_2, such as CO, hydrocarbons, and higher alcohols. Therefore, a highly selective catalyst is required to avoid the formation of undesired by-products for methanol synthesis.

2.3.1 Reaction mechanisms of methanol synthesis

According to the different studies,[5,32,134] methanol synthesis over Cu-based catalysts may proceed via three different reversible reaction pathways (figure 4). 1) Formate mechanism: CO_2 reaction with surface atomic H yields formate as an intermediate, 2) RWGS mechanism with carboxyl intermediate and 3) CO_2 hydrocarboxyl mechanism with $*C(OH)_2$ as intermediate. All three mechanisms lead to the formation of formyl (H_2CO*) which is hydrogenated to methoxy (H_3CO*) and methanol (CH_3OH). During the formate pathway, chemisorbed formate can be formed from CO_2 reaction with dissociated surface hydrogen. Then, surface-bound formate is hydrogenated, which is the rate-determining step, to

produce dioxomethylene that can lose oxygen with the formation of formaldehyde or lose hydroxyl and form H_2CO*. H_2CO* can be further hydrogenated to methoxy and methanol. The RWGS mechanism involves the formation of CO* through the loss of hydroxyl from hydrocarboxyl. HCO intermediate is then hydrogenated to formyl that leads to methanol. The hydrocarboxyl pathway assumes that hydrocarboxyl can be hydrogenated to form COOH* which may subsequently lose hydrogen to form *COH. *COH is then hydrogenated to hydroxymethylene.

Figure 4 Possible mechanism and intermediates of methanol synthesis via CO_2 hydrogenation according to different studies[18,134,135] a) formate mechanism, b) RWGS mechanism, c) hydrocarboxyl mechanism

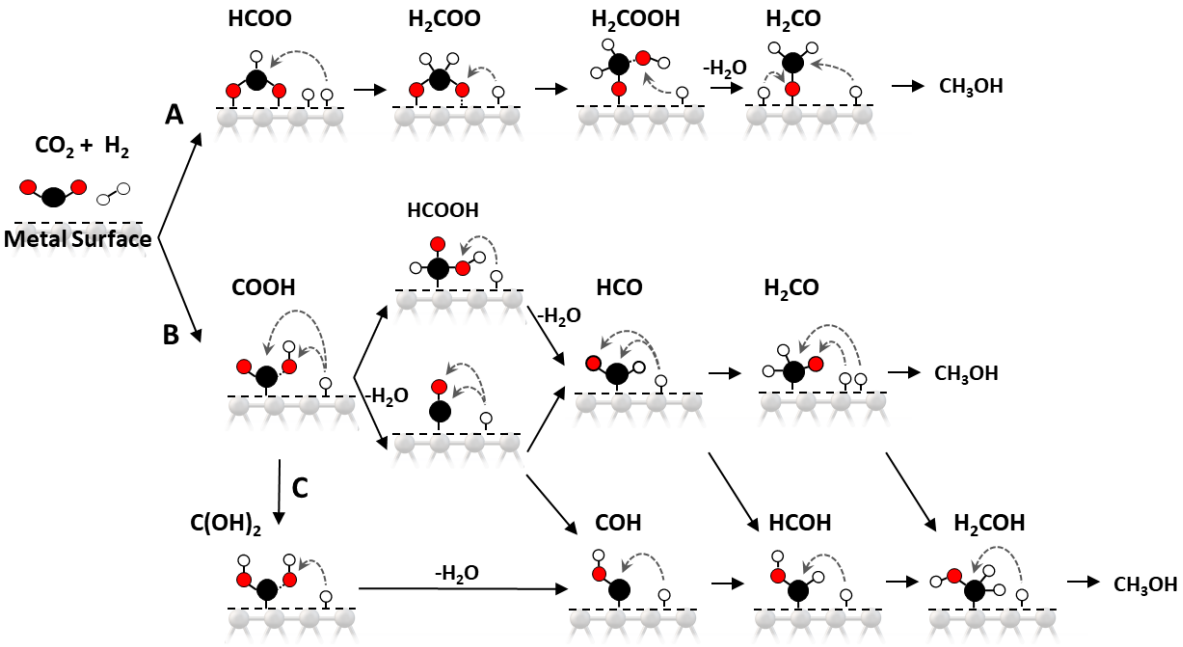

Several studies suggest that formate mechanism leads to a dead end since formaldehyde has not been detected as a side product from methanol synthesis.[134] Some studies present that formate has not been converted to methanol via direct hydrogenation and is rather a spectator species.[5,134,136,137] The kinetics of formate hydrogenation also did not correlate with those of the formation of methanol.[134,138] According to the Wu et al.[134] the RWGS route is questionable as well and methanol formation seems to proceed via hydrocarboxyl route. Based on prior tracer and isotopic labelling studies in conjunction with extensive DFT calculations now available, the CO produced from the fast RWGS reaction was proven not to undergo subsequent H insertions/hydrogenations, on account of the poor stability of the surface HCO that is extremely reactive surface species, with infinitesimally small surface coverages, under integral conditions.[24]

2.3.2 Catalysts used in methanol synthesis

Most used catalyst remains Cu together with different promoters (Zn, Zr, Ce, Al, Si, V, Ti, Ga, B, Cr, etc.).[32] A proper support not only affects the stabilization and formation of the catalysts active phase, but it is also able to control the interaction between the promoter and major component. Additionally, acidity and basicity characteristics of the catalyst are also determined by the selected support.[23]
Low-pressure methanol synthesis relies almost on catalysts based on copper, zinc oxide, and alumina, which acts as a promoter in this catalyst rather than as a classical support.[139] However, $Cu/ZnO/Al_2O_3$ catalysts suffer from the limited selectivity (<70%) for methanol and stringent reaction conditions (50–

100 bar, 200–300 °C).[140] Allam et al.[141] evaluated the improvement of Cu- and Zn- based binary ($CuO-CeO_2$, $ZnO-CeO_2$) and ternary ($CuO-ZnO-CeO_2$, $CuO-ZnO-Al_2O_3$) catalysts for CO_2 hydrogenation to methanol in terms of metal oxide dispersion and morphology. Ternary catalysts prepared by polyol method exhibited a higher activity (about 20%) and selectivity (<65%). Many studies investigate the use of different promoter than ZnO in Cu-based catalysts. According to the Bhanage et al.[125] the CeO_2 has stronger basic sites than ZnO and may be a promising promoter. Wang et al.[125] studied the effect of Cu-based catalysts supported on CeO_2 and ZrO_2 between 200 and 300°C. The CO_2 conversion improved with increasing temperature and selectivity towards methanol was generally higher with Cu/CeO_2 catalyst with highest values at 220°C (>80%). Also Li et al.[142] synthesized mesostructured Cu/AlCeO catalysts with CO_2 conversion up to 22.5% at 553 K and 94% selectivity at 473 K. The studies show that CeO_2 exhibits great performance not only in RWGS reaction but also in methanol synthesis.

Although the most used catalyst is Cu, there are still open questions rising about the active sites. One have suggested that metallic copper is the active site and addition of oxides would sustain the large copper surface and reduce CuO to metallic copper.[36,143] Other suggested the effect of “Cu-Zn” synergy for being essential for the active site[144,145] where methanol is synthesized over Cu^+ at the Cu/ZnO interface, or over Cu cations that dissolve in the ZnO matrix and metallic copper only promotes the dissociation of H_2. According to the Behren’s et al.[146] results where they combined experimentally obtained data with DFT calculations for studying the active sites of methanol synthesis over $Cu/ZnO/Al_2O_3$ industrial catalyst, the most active surface was found to be a Cu step with Zn alloyed into it. The reason for this discussion is the difficulty of obtaining data for the industrial $Cu/ZnO/Al_2O_3$ catalysts under realistic working conditions and the variety of different Cu-based catalysts showing contradicting behaviour.[147]

Other most examined catalysts for CO_2 hydrogenation to methanol are Pd-based catalysts. Pd possesses the ability to activate hydrogen gas into H-adatoms that can spillover unto metallic oxide supports and in the presence of CO (originated from dissociative adsorption of CO_2) form a formate ion which can be further hydrogenated to methanol or methane.[42] The simplest example is Pd supported on ZnO and reduced with temperature >~300°C which results in the formation of the 1:1 PdZn alloy that shows very good selectivity to methanol.[148] From the computational point of view this shows that DFT calculations are very necessary in studies of transition metals and bimetallic systems.

2.4 Synthesis of formic acid

The direct synthesis of formic acid from CO_2 potentially represents a vector for hydrogen storage with promising energy storing capacity (53 $g.l^{-1}$), which exceeds pressurized H_2 tanks (39.4 $g.l^{-1}$ at 700 bar).[149–152] However, the CO_2 reduction reaction is energetically hampered and a serious practical difficulty lies in the low thermodynamic stability of formic acid and fast decomposition kinetics.[152]

2.4.1 Reaction pathways in formic acid synthesis

Recent studies[34,36,153,154] show that CO_2 hydrogenation to formic acid may undergo two different pathways which include formate as an intermediate and depend on the adsorption of the CO_2 molecule. The first pathway is depicted in figure 5 and displays the formation and reaction of monodentate formate with dissociated hydrogen. In the second pathway the bidentate formate is generated and then hydrogenated to produce formic acid.

The direct catalysed hydrogenation CO_2 to HCOOH is thermodynamically disfavoured (ΔG^0_{298}= +33 $kJ.mol^{-1}$) and even under favourable conditions, namely H_2O solvent and low temperatures, very high CO_2/H_2 pressures must be used to reach a limited HCOOH equilibrium concentration.[155] To make the hydrogenation more selective towards the formic acid formation the addition of base is usually employed. Inorganic base generates formate which is then converted to formic acid using a strong acid

and organic base which regenerates formic acid and shifts the reaction equilibrium towards higher selectivity to formic acid.[156] Alternatively, the use of buffers,[157] basic ionic liquids[149] and basic and coordinating solvents (DMSO)[158] is an interesting approach to generate free formic acid to avoid the need to use stoichiometric amounts of an amine or other strong bases as co-reagents.[157] Also reactive distillation is not necessary to form formic acid from formate adducts during product isolation.[149]

2.4.2 Catalytic CO_2 hydrogenation to formic acid

The most commonly used catalysts for the conversion of CO_2 into formic acid are precious metals Rh,[159,160] Ru,[161] Ir,[160,162] Pd[163] as they contain homogeneous ligands, such as phosphine ligands,[164] pincer ligands,[164] N-heterocyclic carbene ligands,[164] proton-responsive ligands.[165,166]
However, the synthesis of these homogenous catalysts is complicated along with high energy consumption.[40]

FIgure 5 Synthesis of formic acid under basic conditions: a) formation of monodentate HCOO intermediate, b) formation of bidentate HCOO intermediate.

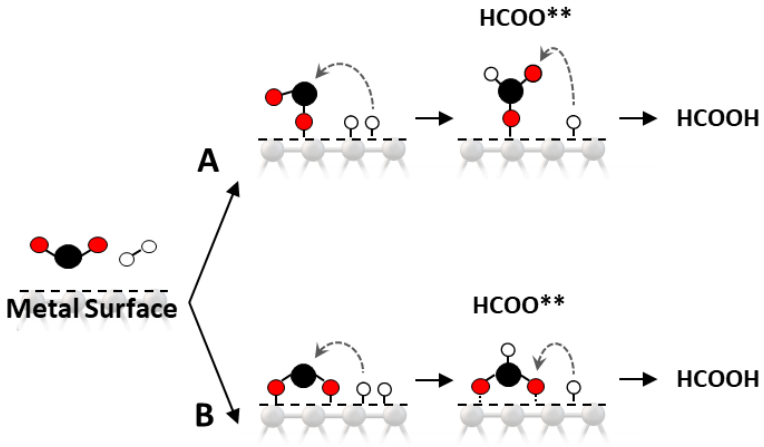

3. Modelling Catalyst Surfaces

Understanding the nature of the active sites, for example, on which and what type of catalysts does the reaction of CO_2 and hydrogen take place, and the reasons for such mechanistic differences among the metals is crucial in the effort to gain a mechanistic interpretation of CO_2 activation, and detailed analysis by the theory are required to link the different prevalent mechanisms on the metals to specific properties at the atomic scale.[167,168] Many DFT studies are aimed on the CO_2 adsorption and H_2 dissociation on the specific pure metal surfaces and their comparison with the previous studies with the intention of finding the mechanism of CO_2 conversion. However, results of quantum calculations are scattered among various papers with the use of different approaches, often mentioned between experimental results without an effort to establish a systematic approach which would make orientation more readable.
Consequently, the aim of this chapter is to summarize and systematise the results of the DFT investigations for the individual transition metal surfaces used in the synthesis of different chemicals from CO_2 hydrogenation.

3.1. Surface energy of transition metal facets

Different facets of catalysts possess unique geometric, electronic structure and thermal stability which may prolong the catalyst durability and increase the product selectivity. The surface energy has an influence on physico-chemical properties, such as the surface tension, strain, etc. It is well-known that

these properties are crucial in the catalytic performance of the materials.[169,170] For example, using DFT with RPBE functional Li et al.[171] found that surface tension affects the reactivity of metal nanoparticles. They studied adsorption energies of oxygen on Au and Pt clusters with 3 nm diameter and found that surface tension of the clusters induces a compression, which weakens the bonding of adsorbates compared with the bonding on extended surfaces. The effect is largest for close-packed surfaces and almost nonexistent on the more reactive steps and edges. The effect is also largest at low coverage and decreases at higher coverages where the strain changes from compressive to tensile. According to them this has direct quantitative relevance to understanding reactions on small particles.

There are many different values of surface energies calculated using different functionals (Table 3) although, the values generally are similar for individual metal. Many studies use PBE functional to calculate surface energies are calculated by PBE functional, however Waele et al.[172] stated that GGA-PBE significantly underestimates the surface energy for materials with a large correlation energy while LDA provides satisfactory results. The surface energy of different metal facets typically decrease in the order of $\gamma\{111\} < \gamma\{100\} < \gamma\{110\}$ and surface with the lowest surface energy is the most thermodynamically stable surface. From the 3d metals the lowest surface energy has Cu surface, from 4d metals it is Ag and from 5d metals the lowest surface energy has Au. The highest surface energy from 3d, 4d and 5d metals has Fe, Rh and Ir, respectively. For Fe surface with bcc structure the surface energy decrease in opposite order as the surface energy of fcc structures.

Figure 6 Physisorbed and chemisorbed CO_2 on metal surface: a) physisorbed CO_2, b) and c) chemisorbed CO_2 with O-down configuration, d) chemisorbed CO_2 with C-down configuration, e) chemisorbed CO_2 with mixed configuration.

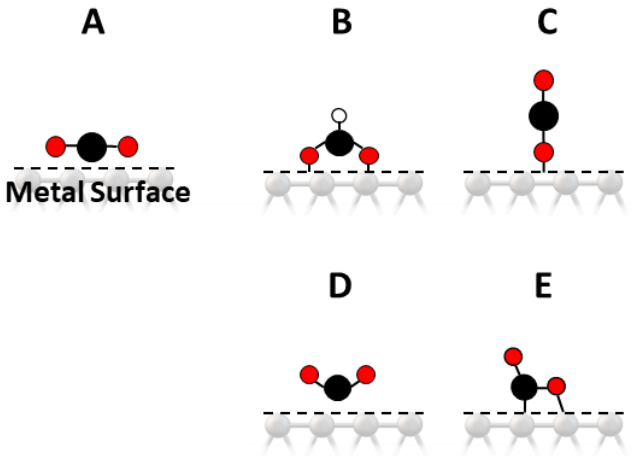

The most favourable facets are the (110) facet for a body-centered cubic (bcc) metal and the (001) facet for a hexagonal close-packed (hcp) metal. However, the low index surfaces are frequently studied due to the fact, that the majority of facets have low surface energy and transition metal nanoparticles are mostly bounded by low-index facets.[173] Also, small nanoparticles, especially clusters, may differ from larger ones, as they expose a higher fraction of coordinatively unsaturated surface atoms in the form of corner and edge atoms. The lower coordinative unsaturation may lead to narrowing of the d-band, which results in an upward shift of the band's energy and, consequently, in stronger adsorption of reaction intermediates.[174] Therefore, DFT studying of CO_2 molecule activation, adsorption and dissociation together with hydrogenation on different low index surfaces is very important for understanding the catalytic activity and reaction mechanism and for development of new nano-catalysts.

10.1002/cctc.201901879

Table 3. Comparison of the calculated surface energies by DFT, FCD and MAEAM method for most commonly used metals in CO_2 hydrogenation

Group	Metal	Plane	LDA	GGA	PW91	PBE	PBEsol	SCAN	SCAN+rV10	FCD	MAEAM
3d metals	Fe	111	1	-	2.08[175]	2.10[175], 2.58[176]	-	-	-	2.73[177]	-
		100	-	2.5[178]	2.13[175]	2.15[175], 2.47[176]	-	-	-	2.22[177]	-
		110	-	2.45[178]	2.25[175]	2.27[175], 2.37[176]	-	-	-	2.43[177]	-
		211	-	-	-	2.5[176]	-	-	-	2.59[177]	-
	Ni	111	-	1.92[178]	-	-	-	-	-	2.01[177]	1.17[179]
		100	-	2.22[178]	-	-	-	-	-	2.43[177]	1.31[179]
		110	-	-	-	-	-	-	-	2.37[177]	1.42[179]
		211	-	-	-	-	-	-	-	-	1.37[179]
4d metals	Cu	111	1,81[180]	1.3[178]	-	1.33[180], 1.94[181]	1.59[180]	1.49[180]	1.74[180]	1.95[177]	0.94[179]
		100	1.99[180]	1.44[178]	-	1.48[180], 2.15[181]	1.76[180]	1.71[180]	1.91[180]	2.17[177]	1.01[179]
		110	2.13[180]	-	-	1.63[180], 2.19[181]	1.88[180]	1.84[180]	2.02[180]	2.24[177]	1.11[179]
		211	-	-	-	2,1[181]	-	-	-	-	1.08[179]
	Rh	111	2.67[180]	2.01[178]	-	2.09[180], 2.61[181]	2.40[180]	2.33[180]	2.61[180]	2.47[177]	1.83[179]
		100	3.04[180]	2.35[178]	-	2.77[180], 3.01[181]	2.97[180]	2.71[180]	3[180]	2.8[177]	2.14[179]
		110	2.86[180]	-	-	2.55[180], 3.08[181]	2.77[180]	2.76[180]	2.82[180]	2.9[177]	2.27[179]
		211	-	-	-	3[181]	-	-	-	-	2.18[179]
	Pd	111	1.88[180]	1.33[178]	-	1.36[180], 1.90[181]	1.63[180]	1.54[180]	1.77[180]	1.92[177]	0.93[179]
		100	2.43[180]	1,51[178]	-	1.79[180], 2.15[181]	2.15[180]	2.03[180]	2.29[180]	2.23[177]	1.02[179]
		110	2.25[180]	-	-	1.61[180], 2.23[181]	1.93[180]	1.83[180]	2.05[180]	2.32[177]	1.12[179]
		211	-	-	-	2.15[181], 1.15	-	-	-	-	1.08[179]
	Ag	111	1.13[180]	0.76[178]	-	0.78[180], 1.27[181]	1[180]	0.97[180]	1.16[180]	1.17[177]	0.71[179]
		100	1.16[180]	0.84[178]	-	0.81[180], 1.27[181]	1.04[180]	1[180]	1.18[180]	1.2[177]	0.75[179]
		110	1.32[180]	-	-	0.93[180], 1.35[181]	1.19[180]	1.12[180]	1.33[180]	1.24[177]	0.83[179]
		211	-	-	-	1,3[181]	-	-	-	-	0.82[179]
5d metals	Ir	111	-	2.06[178]	-	2,77[181]	-	-	-	2.97[177]	2.04[179]
		100	-	2.84[178]	-	3,49[181]	-	-	-	3.72[177]	2.57[179]
		110	-	-	-	3,53[181]	-	-	-	3.61[177]	2.66[179]
		211	-	-	-	3,32[181]	-	-	-	-	2.5[179]
	Pt	111	1.98[180]	1.49[178]	-	1.56[180], 2.0[181]	1.85[180]	1.64[180]	1.89[180]	2.29[177]	0.9[179]
		100	2.35[180]	1.85[178]	-	1.88[180], 2.4[181]	2.21[180]	2.04[180]	2.25[180]	2.73[177]	1.08[179]
		110	2.46[180]	-	-	1.94[180], 2.5[181]	2.31[180]	2.08[180]	2.32[180]	2.82[177]	1.19[179]
		211	-	-	-	2,22[181]	-	-	-	-	1.11[179]
	Au	111	1.24[180]	0.71[178]	-	0.75[180], 1.14[181]	1.1[180]	0.93[180]	1.17[180]	1.28[177]	0.64[179]
		100	1.39[180]	0.86[178]	-	0.86[180], 1.36[181]	1.13[180]	1.05[180]	1.24[180]	1.63[177]	0.71[179]
		110	1.61[180]	-	-	0.99[180], 1.41[181]	1.26[180]	1.2[180]	1.47[180]	1.7[177]	0.79[179]
		211	-	-	-	1,29[181]	-	-	-	-	0.76[179]

3.2 CO_2 adsorption behaviour on solid surfaces

The first step of CO_2 activation and dissociation is its adsorption on the catalyst metal surface. In CO_2 hydrogenation, the interaction between hydrogen and the metal surfaces is a crucial part. An appropriate H_2 and CO_2 co-adsorption equilibrium will strongly affect the reaction.[182] Different computational studies investigated the most stable adsorption structures of CO_2 on metal surfaces. Burghaus[183] summarised possible adsorption structures of physisorbed CO_2 conformations, where CO_2 is adsorbed linearly, parallelly or upright on the surface and weakly chemisorbed CO_2 where CO_2 can be adsorbed in a carbon-atom-down, carbon-atom-up and mixed position (Figure 6). Various sites may be populated simultaneously with a population distribution depending on the surface temperature.
The effect of the surface can be also examined with DFT calculations. The adsorption may occur on different sites of fcc, namely 111, 110, 111 and 211 facets (Figure 7). CO_2 can be adsorbed on a 3-fold hollow site in the empty space between 3 metal atoms, on a 4-fold hollow site in the empty space between 4 metal atoms, on a bridge site (long or short) where 2 metal atoms are positioned next to each other and on the top site of the metal surface. Possible adsorption sites are depicted in Figure 7 for fcc 111, 100, 110 and 211 transition metal surfaces.

Figure 7 Possible surface adsorption sites of fcc 100, 110, 111 and 211 transition metal surfaces examined by computational studies.

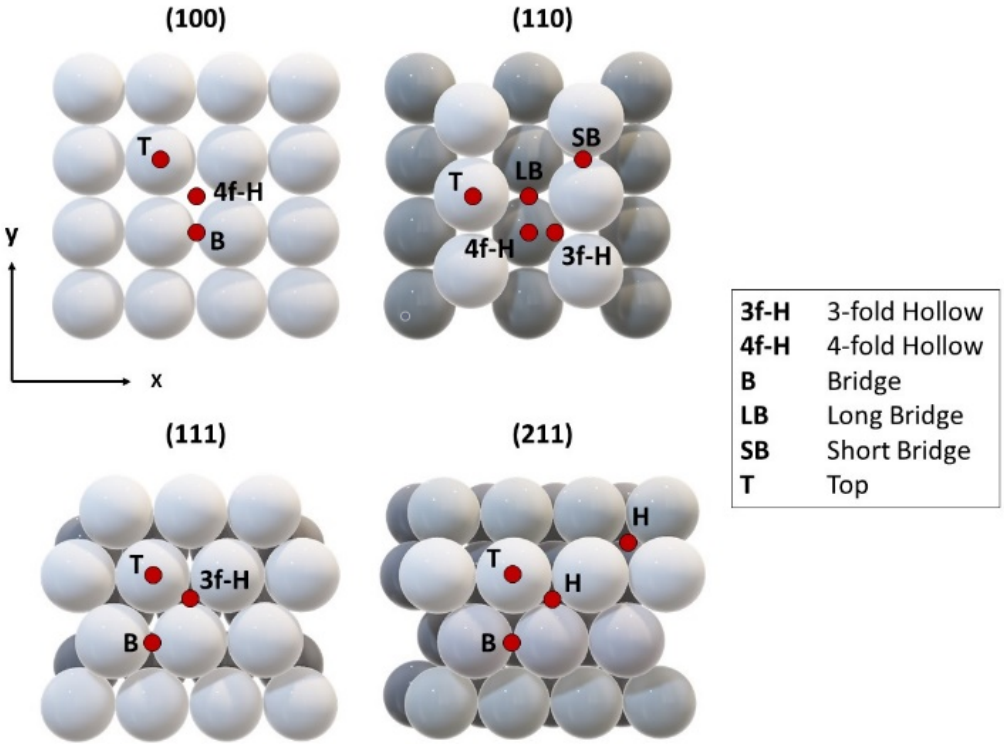

The adsorption energies calculated computationally with the use of different functionals is shown in Table 4. The adsorption energies were mostly calculated with PBE functional. The presented values do not show adsorption free energies which values depend on the temperature and are >1 eV higher than adsorption energy. It can be observed that Fe surfaces have the lowest adsorption energy and it seems that the adsorption of CO_2 is strongest from selected transition metal surfaces. At the present, only few articles show DFT calculated values of adsorption energy for transition metals. Besides, for various surfaces the adsorption energy values are not consistent between different articles and show negative and positive values. Liu et al.[173] used GGA and PAW potentials which resulted in negative values of adsorption energies. However, the values calculated by Wang[184] and Muttaqien et al.[185]

using PBE functional with Vanderbilts ultrasoft pseudopotentials and vdW-DF functional respectively, are positive. This indicates that the interaction with the surface is repulsive and positive numbers are due to artefacts of the DFT calculations as they are a local minimum that has no meaning. Hence, more calculations are essential to prove the adsorption energy values calculated by DFT since the use of different functionals and potentials leads to incoherent adsorption energy values which report completely different results and therefore show various processes taking place on transition metal surfaces. The adsorption energy calculated for Ni surfaces by Czelej et al.[186] decrease in order Ni(111) > Ni(100) > Ni(110) and for Cu surfaces adsorption energy calculated by Wang et al.[184] increases from Cu(111) < Cu(100) < Cu(110). For 4d and 5d metals, the adsorption energy is weaker across the different planes analysed. It is important to note that for these metals more computational studies of adsorption energies would be also desired to be able to draw meaningful conclusions.

Table 4 Comparison of the adsorption energies of the most favourable adsorption sites for CO_2 species in different surfaces

			Adsorption energy [eV]		
Group	Metal	Plane	PBE	rPBE	PBE+vdW
3d metals	Fe	111	-1.35[156]	-1.11[157]	-
			0.078[149]	-1.109[158]	-
		100	-1.47[149]	-	-
			-1.45[159]	-	-
			-1.08[156]	-	-
			-0.92[151,160]	-	-
		110	- 0.56[149]	-	-
			-0.54[161]	-	-
	Ni	111	-0.02[149]	-	-0.18[155]
		100	-0.052[149]	-	-0.65[155]
		110	-0.52[149]	-	-0.77[155]
			-0.33[162]	-	-
	Cu	111	-0.034[149]	-	-
			0.2[153,154]	-	-
		100	-0.056[149]	-	-
			0.23[153]	-	-
		110	0.33[153]	-	-
4d metals	Rh	111	0.24[149]	-	-
		100	-0.36[149]	-	-
			-0.70[163]	-	-
	Pd	111	0.3[149]	-	-
	Pd	100	-0.057[149]	-	-
	Ag	111	-0.035[149]	-	-
		100	-0.04[149]	-	-
5d metals	Ir	111	0.3[149]	-	-
		100	-0.29[149]	-	-
	Pt	111	0.39[149]	-	-
		100	-0.043[149]	-	-

Au	111	-0.033[149]	-	-
	100	-0.038[149]	-	-

3.3 The accuracy of the DFT using various functionals

When comparing the simulations to experiments there is additionally the uncertainty of whether one picked the correct experimental structure to simulate, for example the structures of the metal surfaces, the adsorption sites, and the adsorbate coverage ratio. There is also uncertainty in the measurement of the adsorption energies due to the possible surface defects.

3.3.1 Performance of DFAs for gas phase reaction energetics

Several scientists worked on the compilations of experimental data of adsorption reactions to compare them with values obtained by using different functionals. Every functional is used for different purposes and provides different values. The only specifically designed functionals to treat adsorption energies are RPBE and BEEF-vdW[187], although there are many other functionals that have general-purpose and may provide good values.

The first databases with experimental adsorption energies reported for the purposes of benchmarking DFT have been proposed by Hammer et al.[188] which included 5 chemisorption energies for CO adsorption and Wellendorff et al.[189] that included 10 chemisorption energies for CO adsorption and 8 energies for H_2 adsorption on different transition metals. However, Wellendorff et al.[190] subsequently discovered that several of these energies had large calibration errors or were invalid and therefore they refined the tables and compiled an experimental database for 39 different adsorption reactions occurring on 10 different transition metal surfaces. They divided adsorption reactions into a) adsorbate-surface interactions characterized by strong covalent bonds and b) the adsorbate-surface or adsorbate-adsorbate bonding with large van der Waals contributions to the total adsorbtion energies. Chemisorption energies were compared to the theoretical results computed by six DFT functionals, namely LDA, PBEsol, PW91, PBE, RPBE and BEEF-vdW. According to their benchmarks errors of chemisorbed systems of the various functionals decrease from LDA > PBEsol > PW91 > PBE > RPBE > BEEF-vdW. PBE functional that was shown in Table 4 to be used extensively for calculations of adsorption energies in different studies overbinds, but performs somewhat better than functionals LDA, PBEsol and PW91, whereas both RPBE and BEEF-vdW that have been fitted to describe surface adsorbate bonds performs best. The experimental and theoretical values are shown in Table 5.

There is no well-defined way to know what contribution to the adsorption energy really comes from van der Waals interactions and therefore it is not exactly know how to classify surface reactions into the two classes provided by Wellendorff et al.[187,190] Different division of the experimental database was proposed by Duanmu et al.[187] They divided experimental database to open-shell radical adsorption processes (adsorption of H atoms on metal surface) and closed-shell molecular adsorption processes (adsorption of CO molecule on metal surface). The adsorption energies were recalculated with PBE and

Table 5 Comparison of experimental and theoretical energy values of chemisorption reactions upon gas adsorption, in kJ/mol according to different studies

Type	Reaction	Coverage	Experimental data[187,190]		LDA[190]	PBEsol[190]	PW91[190]	PBE[190]	PBE[187]	PBE[191]	RPBE[190]	RPBE[191]	BEEF-vdW[190]	BEEF-vdW[191]	M06-L[187]	GAM[187]	MN15-L[187]	RPA[191]
Adsorption reaction	CO + Ni(111) → CO/Ni(111)	1/4	-119	-124	−268	−221	−177	−175	-185	-	−140	-	−146	-	-131	-217	-	-
	CO + Pt(111) → CO/Pt(111)	1/4	-117	-124	−213	−184	−156	−156	-162	-161	−136	-124	−133	-115	-141	-135	-131	-131
	CO + Pd(111) → CO/Pd(111)	1/4	-139	-144	−268	−229	−188	−175	-196	-183	−153	-142	−156	-143	-164	-174	-152	-152
	CO + Pd(100) → CO/Pd(100)	1/4	-151	-157	−255	−217	−181	−164	-184	-	−154	-	−150	-	-165	-162	-	-
	CO + Rh(111) → CO/Rh(111)	1/4	-135	-142	−244	−214	−185	−184	-183	-184	−163	-150	−162	-144	-162	-169	-134	-134
	CO + Ir(111) → CO/Ir(111)	1/4	-155	-164	−244	−216	−190	−189	-190	-203	−169	-167	−170	-165	-192	-182	-142	-142
	CO + Cu(111) → CO/Cu(111)	1/4	-52	-57	−132	−103	−75	−73	-72	-71	−56	-39	−55	-43	-58	-49	-24	-24
	CO + Ru(001) → CO/Ru(001)	1/4	-154	-161	−240	−212	−184	−182	-186	-	−162	-	−162	-	-169	-163	-	-
	CO + Co(001) → CO/Co(001)	1/4	-112	-119	−234	−193	−162	−148	-160	-	−137	-	−138	-	-168	-128	-	-
	H + Pt(111) → H/Pt(111)	1/4	-265	–	–	–	–	–	-260	-	-250	-	-249	-225	-	-	-	-
	H + Ni(111) → H/Ni(111)	1/4	-279	–	–	–	–	–	-272	-	-243	-	-311	-260	-	-	-	-
	H + Ni(100) → H/Ni(100)	1/4	-273	–	–	–	–	–	-268	-	-247	-	-255	-211	-	-	-	-
	H + Rh(111) → H/Rh(111)	1/4	-265	–	–	–	–	–	-272	-	-263	-	-256	-226	-	-	-	-
	H + Pd(111) → H/Pd(111)	1/4	-274	–	–	–	–	–	-272	-	-259	-	-250	-200	-	-	-	-
Surface Reaction	H_2 + Pt(111) → 2H/Pt(111)	1.8	-70	–	−160	−129	−94	−79	–	–	–	−66	−48	21	-	-	-	-
	H_2 + Ni(111) → 2H/Ni(111)	1/8	-91	–	−184	−144	−107	−104	–	–	–	−79	−64	17	-	-	-	-
	H_2 + Ni(100) → 2H/Ni(100)	1/8	-91	–	−182	−145	−102	−85	–	–	–	−68	−56	17	-	-	-	-
	H_2 + Rh(111) → 2H/Rh(111)	1/8	-67	–	−180	−148	−112	−112	–	–	–	−84	−67	15	-	-	-	-
	H_2 + Pd(111) → 2H/Pd(111)	1/8	-85	–	−184	−151	−116	−91	–	–	–	−88	−67	18	-	-	-	-

previously untested M06-L, GAM and MN15-L functionals were applied for same transition metal surfaces. The results shown in Table 5 were compared with the values calculated by Wellendorff et al.[190] They found that BEEF-vdW, GAM, RPBE, and M06-L are best performing functionals for open shell radical adsorption processes while MN15-L, followed by BEEF-vdW, M06-L, and GAM are the best for closed-shell molecular adsorption processes (Table 6).

Overall, literature shows that relatively good performance can be provided by BEEF-vdW, M06-L, GAM, MN15-L and RPBE functional which makes them good candidates for application to heterogeneous catalysts.

A different type of benchmark database was provided by Schmidt et al.[191] from many-body perturbation theory. They used RPA to construct and calculate 200 different full coverage adsorption reactions including OH, CH, NO, CO, N_2, N, O, and H adsorbed on transition metals. The high coverage was used due to the large computational cost of the calculations. They also calculated 5 adsorption energies for CO and 2 adsorption energies for H_2 at experimentally relevant coverage listed in Table 5 and surface energies. The RPA was compared to LDA, PBE, RPBE, vdW-DF2, mBEEF, BEEF-vdW and MBEEF-vdW. RPA was found to perform as well as the GGA and van der Waals density functionals RPBE and BEEF-vdW for adsorption and it outperformed all DFT functionals for surface energies. The problem of RPA is high computational cost since the method is computationally much more demanding. With high coverage the problem can be overcomed and RPA results can be compared with experimental data of reactions taking place at high gas pressure conditions.

Table 6 Comparison of the mean signed errors and mean unsigned errors for each functional according to the Duanmu et al.[187]

Open-shell reactions			Closed-shell reactions		
Functional	MUE	MSE	Functional	MUE	MSE
BEEF-vdW1	6,5	1,6	MN15-L	4,1	0,2
GAM	7,5	2,8	1 BEEF-vdW	5,2	2,9
1 RPBE	8,2	2,6	M06-L	5,5	2
M06-L	8,8	2,9	GAM	9	4,8
PW911	9,4	−5.5	RPBE1	9,1	7,4
PBE	9,9	−5.6	PW911	9,3	2,7
MN15-L	10,4	0,4	PBE	9,4	2,3
PBEsol1	15,3	−14.2	PBEsol1	9,8	−3.9
LSDA1	26,8	−26.8	LSDA1	13,5	−12.7

3.3.2 Dispersion forces

BEEF-vdW functional in presented papers with best values of adsorption energy showed that van der Waals correction advance theoretical data towards experimental values of adsorption energy and therefore displays that dispersion forces may play an important role. This may be also the reason for the high errors in benchmark database for LDA functional. Dispersion forces are the result of correlation between zero-point fluctuations of the dipole moments of atoms, molecules, etc. long distanced from each other. The conventional semi-local XC functionals, such as LDA, are very local and cannot capture long-range correlations.

Another study that examines the results of CO_2 hydrogenation using functionals including van der Waals forces was done by Studt et al.[192] They performed DFT calculations for CO and CO_2 hydrogenation on Cu(211) using RPBE and BEEF-vdW functional. BEEF-vdW functional resulted in quite different results where intermediates and transition-states involved in CO_2 hydrogenation interacted considerably stronger with Cu(211) surface in comparison with RPBE functional. Therefore Studt et al. suggested that a functional explicitly including van der Waals interaction is needed to get the details of selectivity in CO_2 hydrogenation correctly.

Tameh et al.[143] examined the accuracy of DFT for prediction of kinetics in CO_2 hydrogenation to methanol using microkinetic modelling. They compared RPA method to different functionals including RPBE and BEEF-vdW functionals. BEEF-vdW functional predicted that hydrogenation of CO_2 is thermodynamically favourable which they explained by their errors treating the OCO backbone. However, RPA also provides a description of the vdW interaction. Tameh et al. also found different results in the case of including dispersion forces. Their PBE results suggested that metallic copper is not the active site for CO_2 hydrogenation in industrial methanol synthesis while RPA predicted that metallic copper is still a possible active site for catalysing CO_2 hydrogenation.

3.3.2 DFAs reliability for activation barriers on transition metal surfaces

While the DFT functionals have been extensively studied in calculations of adsorption and surface energies, their reliability for activation barriers on surfaces is not well understood. Sharada et al.[193] proposed an experimental database consisting of accurate barriers for dissociation reactions of molecules on transition metals. The BEEF-vdW GGA outperformed the MS2 meta-GGA and HSE06 hybrid, in direct contradiction to the gas phase barrier accuracies of these functionals. Therefore, the key driver for functional is the description of surface-adsorbate interactions, and not charge separation or self-correction. Sharada et al. stated that that transition states for dissociative adsorption closely interact with surface, while gas phase transition states are relatively isolated species.

3.3. Recent DFT calculations of the most commonly used metal surfaces

A systematic review of the literature regarding the mechanism of CO_2 hydrogenation on various metal surfaces is presented in this section. The critical discussion is based on data about adsorption and surface energies. Furthermore, it is focused on the different metal crystallographic sites and their surface interactions with CO_2 that leads to various intermediates. The section also discusses the role of microkinetic modelling in obtaining information about reaction mechanism of CO_2 hydrogenation.

3.3.1 Fe catalytic surfaces

DFT calculations were carried out for CO_2 adsorption on Fe(100), (110), (111) and (211) surfaces. Also, several studies examined H_2 adsorption and dissociation on Fe surfaces to determine the most effective H_2:CO_2 ratio for the activation of the reagents.

In RWGS reaction: Wang et al.[194] investigated the adsorption dissociation and hydrogenation of CO_2 on fcc Fe(100), (110), (111) and (211) facets with the use of GGA with the PBE functional and with the use of PAW pseudo-potentials. They suggested that the Fe facet plays an important role in impacting the formation of key intermediates and thus altering the preferred pathways for CO_2 conversion. The results indicated that an appropriate H_2-CO_2 co-adsorption equilibrium is important for effective activation of the reactants. Energetically most favourable for CO_2 adsorption was Fe(111) and (211) facet (Figure 8). During the dissociation and hydrogenation of CO_2, the Fe(111) favoured associative pathway with the HCOO* formation due to a relatively lower kinetic barrier while the (100) and (110) facets were more selective to redox pathway with CO* formation. The Fe(211) exhibited a competitive preference for the formation of CO* and HCOO*. All these Fe surfaces did not favour the formation of COOH* intermediate. Liu et al.[195] examined the adsorption and decomposition of CO_2 on transition metal fcc and bcc (100) surface atoms of Fe, Co, Ni and Cu using PW-DFT. From the cases studied, Fe surfaces were found to be the most favourable for CO_2 adsorption. However, Co and Ni showed favourable thermodynamics and low decomposition barriers for CO_2 reduction. Furthermore, their results showed that different Fe structure (fcc, bcc) affects thermodynamics. Accordingly, Wang el al.[182] investigated the adsorption and activation of CO_2 and H_2 over bcc Fe(100) with PAW pseudo-potentials and GGA approximation with PBE functional. The energetically most favourable adsorption

of CO_2 occurred on the 4-fold hollow site with the C atom sitting in the middle of the 4-fold unit and right above the second layer Fe atom, and the two O atoms bound at the centre of two Fe-Fe bridge bonds. The adsorption energy of this configuration was 0.92 eV. Their calculation results suggest that a moderate H_2 versus CO_2 ratio is likely more suitable to achieve better adsorption and effective activation of the reactants which would facilitate CO_2 hydrogenation.

To understand the abilities of the water-gas shift reaction catalysed by metallic Fe Li et al.[196] carried out calculations of CO and H_2O on clean Fe(110) surface with different CO and H_2O ratios. H_2O dissociative adsorption was found to be very favorable kinetically and thermodynamically, which is necessary for the redox reaction [CO + O → CO_2] and the carboxylic reaction [CO + OH → COOH → CO_2 + H]. The formation of COOH as well as HCO and COH was found to be neither kinetically nor thermodynamically favourable.

Figure 8 Top and side view of the possible most stable a) CO_2 and b) H adsorption structures on the Fe(111), Fe(110) and Fe(211) surfaces [reprinted from[194] with permission from Elsevier].

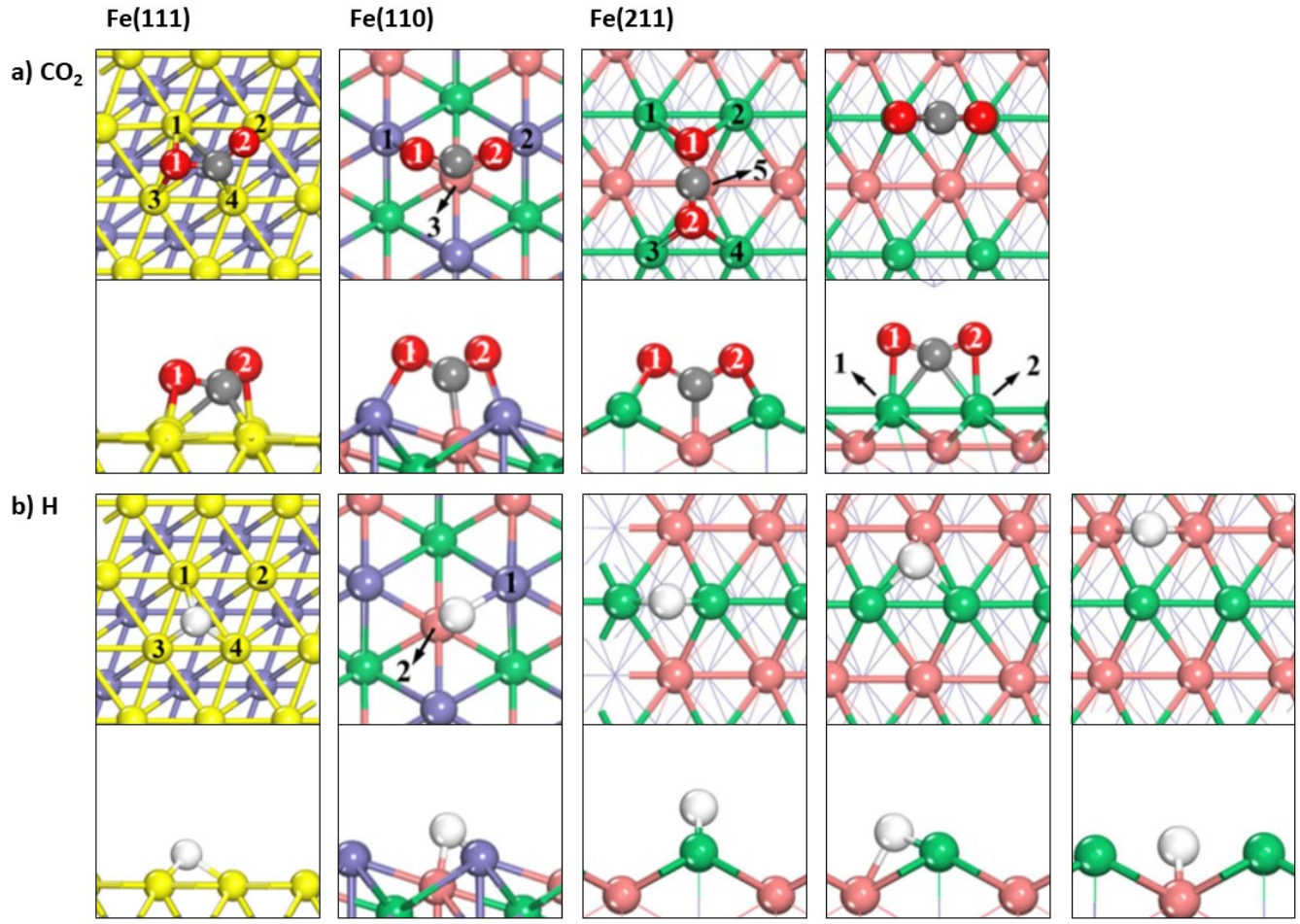

In methanol synthesis: Since CO_2 hydrogenation on Fe surfaces seem to proceed via an associative pathway in RWGS, the formate intermediate may also lead to the production of methanol. Chen et al.[197] studied Fe(111) surface for decomposition of CO_2 with PW-DFT method. Their data show that isomers $FeCO_2$(S-μ_3-C,O,O´), FeCO(S-η1-C) and FeX(T,S- μ_2-X) or FeX(B-μ_3-X), for X = C and O atoms, are energetically favoured among calculated structures of Fe(111)/CO_2, Fe(111)/CO and Fe(111)/X. Their simulations of CO_2 dissociation on Fe(111) surface showed that the catalytic process is likely to proceed via a three-step mechanism. Li et al.[198] with the use of PAW method in conjunction with the rPBE functional studied microkinetic modelling of CO_2 hydrogenation on Fe(111) surface. They

found out that the most probable path for the hydrogenation of CO_2 on Fe(111) surface is the formation of a formate-vertical structure.
Even though these studies show interesting results, they report different structures or do not mention whether the studied Fe surfaces were fcc or bcc structures. Moreover, while there are many DFT studies discussing the effect of Fe on CO_2 conversion the microkinetic calculations were not performed for Fe surfaces.

3.2.2 Ni catalytic surfaces

In methanation: Ren et al.[199] studied the mechanism of CO_2 methanation on the fcc Ni(111) surface using DFT calculations within GGA and PW91 functional. They investigated three mechanisms that fall into two categories: 1) mechanisms including CO intermediate 2) and mechanisms excluding CO intermediate. From the studied mechanisms, the optimal mechanism of CO_2 methanation on Ni(111) included a CO intermediate (figure 9c). CO_2 firstly decomposes into CO and O on the Ni(111) surface. Then CO decomposes into C and O and C hydrogenates to CH_4. The highest barrier of this path was 237.4 kJ/mol from the dissociation of CO into C and O species. Accordingly, the elementary reaction $CO \rightarrow C + O$ was the rate-determining step in this path. To understand the hydrogenation mechanisms for CO_2 on Ni(110) surface kinetic DFT studies have been also performed by Bothra et al.[200] Their calculations using the PWSCF code within the GGA and PBE functional shown that the CO_2 hydrogenation passes via various stable intermediates, namely, carbon monoxide, methoxy, formate and yield the product methane. All three stable (formate, CO_2 or CO) intermediates can be hydrogenated to produce methane. The adsorption and decomposition processes of CO_2 on Ni(110) surface were also examined by Czelej et al.[201] using SP-DFT method and performing CI-NEB calculations. The CO_2 adsorption conformations and adsorption, desorption on Ni(110) surface are displayed in figure 9a and 9b. They gave insight into the CO_2/Ni(110) → CO/Ni(110) + O/Ni(110) reaction mechanism and distinguished two decomposition steps: 1) surface diffusion of CO_2 to the H-2 conformation with (depending on the starting geometry) 1-2 transition states; and 2) breaking of the coordinated C-O bond with total reaction barrier of 0.44 eV.
In methanol synthesis: Maulana et al.[202] recently investigated the CO_2 hydrogenation to methanol on clean Ni(111) and Ni(111)-M (M = Cu, Pd, Pt, Rh) surfaces using DFT and microkinetics. The DFT calculations with PBE functional showed that formate-mediated and carboxyl-mediated pathways depicted in Figure 10 seem to be the main routes for production of methanol. The microkinetic modelling determined that formate route prefers mechanism via HCOOH* intermediate with much higher TOF value than carboxyl route and carboxyl pathway prefers HCO* intermediate. The kinetic performance was increased by Ni catalysts doped with Cu, Pd and Pt for formate mechanism and with Cu, Pt and Rh for carboxyl route at 573 K.
In formic acid synthesis: Ni metal surface was also investigated by DFT calculations to see if the formation of formic acid is also possible on this surface. Peng et al.[34] using DFT-PW91 and CI-NEB calculated activation energy barriers and detailed reaction coordinates for CO_2 hydrogenation to formate, carboxyl and formic acid on Ni(110) surface. They provided insights into the possible role of subsurface H and suggested that transiently energetic subsurface H emerging onto the Ni(110) surface can lead to hydrogenation of formate to formic acid.
Recent studies show that there is still enough space for further computational studies. Microkinetic modelling is lightly used for comprehension of CO_2 conversion of Ni surfaces. Additional DFT calculations in conjunction with microkinetic modelling would bring more information about the Ni(100) and Ni(110) surface elementary steps of CO_2 hydrogenation which are still not clear.

10.1002/cctc.201901879

Figure 9 a) CO_2 adsorption conformations on Ni(100), (110) and (111) surfaces [reprinted from[186] with permission from Elsevier], b) CO_2 adsorption and desorption structures on Ni(110) surfaces and c) CO_2 methanation mechanism on Ni(111) surface [reprinted from[203] with permission from Elsevier].

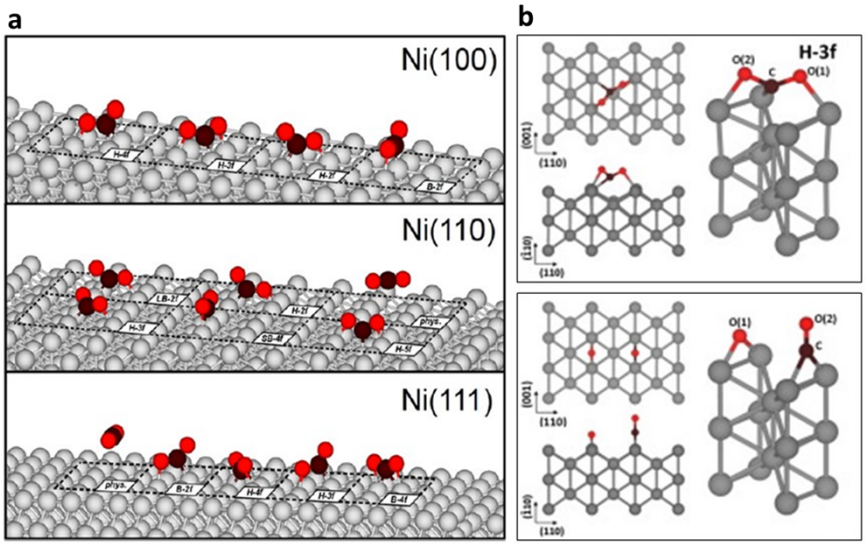

c

$H_2 + 2^* \rightarrow 2H^*$

$CO_2 + * \rightarrow CO_2^*$

$CO_2^* + * \rightarrow CO^* + O^*$

$CO^* + * \rightarrow C^* + O^*$

$C^* \xrightarrow{+H^*} CH^* \xrightarrow{+H^*} CH_2^* \xrightarrow{+H^*} CH_3^* \xrightarrow{+H^*} CH_4 + *$

$O^* \xrightarrow{+H^*} OH^* \xrightarrow{+H^*} H_2O^* \rightarrow H_2O + *$

Figure 10 Proposed reaction pathways of CO_2 hydrogenation to methanol on Ni(111) and Ni(111)-M surfaces. Reproduced from ref. A. L. Maulana, R. I. D. Putra, A. G. Saputro, M. K. Agusta, Nugraha, H. K. Dipojono, *Phys. Chem. Chem. Phys.* **2019**, *21*, 20276–20286 with permission from the PCCP Owner Societes.

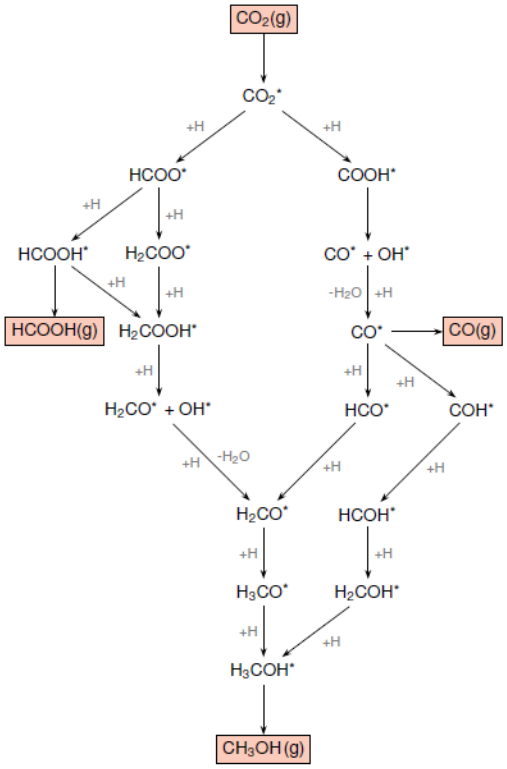

3.3.3 Cu catalytic surfaces

The mechanism of CO_2 hydrogenation to methanol over Cu(111) surface was proposed by many researchers through DFT calculations[22,174,204,205] however, if the active site is metallic Cu or CuZn alloy is still an open question.

In RWGS reaction: Choi et al.[93] studied catalytic behaviour of metal catalysts (Pd, Ni, Cu, Ag) with different facets (100), (110), (111) in high-temperature RWGS reaction. They observed that Cu, Pd and Ni catalysts have higher H adsorption energies and easily produce H-adsorbed species and Ag surface is unfavourable for H adsorption. For all highly activated catalysts, the formate group was an intermediate adsorbed species and Cu, Ni and Pd catalysts can be used to promote RWGS reaction.

In methanol synthesis: Grabow et al.[22] performed DFT and very detailed microkinetic calculations to determine the energetics of 22 surface species and the activation energy barriers and pre-exponential factors for description of 49 elementary surface reactions on Cu(111) by using GGA-PW91 and DACAPO total energy code. According to their results, clean Cu(111) surface does not represent the active site accurately on commercial $CuZnO/Al_2O_3$ catalyst. More suitable for active site representation may be open and partially oxidized Cu facet, e.g., Cu(110), Cu(100) a or Cu(211). They present that CO_2 is hydrogenated via the sequence $CO_2^* \rightarrow HCOO^* \rightarrow HCOOH^* \rightarrow CH_3O_2^* \rightarrow CH_2O^* \rightarrow CH_3O^* \rightarrow CH_3OH^*$. The formation of $HCOO^*$ from CO_2^* and adsorbed H^* is fast and does not require a CO_3^* intermediate. CO hydrogenation yields methanol through the sequence $CO^* \rightarrow HCO^* \rightarrow CH_2O^* \rightarrow CH_3O^* \rightarrow CH_3OH^*$. Studt et al.[147] also performed DFT with BEEF-vdW and microkinetic calculations which showed reasonable reaction barriers for the formate-mediated route which promoted the results of Grabow et al.[22] In combination with their catalytic tests of reduced Cu/MgO and $Cu/ZnO/Al_2O_3$ catalysts at 523 K performed in fixed-bed flow reactor at 30 bar and 503 K they concluded that the catalyst mixture optimizes the reaction kinetics and the feed gas optimizes the equilibrium thermodynamics of the system. In contrast, Zhao et al.[204] by using PAW DFT calculations with PW91 functional and dimer method for examination of various reaction and diffusion pathways stated that CO_2 conversion to methanol on Cu(111) surface does not lead through direct hydrogenation of formate intermediate. Their reason for that are high reaction barriers of HCOO and H_2COO. Models using dimer method showed that hydroxycarbonyl mechanism may be possible, but the H_2O plays a crucial role in hydrocarboxyl mechanism enhancement. Accordingly, the methanol may be produced by CO_2 + 6H + (H_2O) → trans-COOH + 5H → t,t-COHOH + 4H → t,c-COHOH + 4H → c,c-COHOH + 4H → COH + OH + 4H → HCOH + 3H + OH → H_2- COH + 2H + OH → H_3COH+H+OH → H_3COH + H_2O. They also suggest that both RWGS and methanol synthesis from dry CO_2+H_2 mixtures on the clean Cu(111) surface at low temperatures are unlikely because the dominant HCOO surface species is a mechanistic ‘‘dead end’’. The hydrocarboxyl mechanism was suggested also by Yang et al.[205] performing the DFT calculations with the use of PW-GGA approximation in combination with experimental kinetic tests of clean Cu(111) and Cu/ZnO(0001) surfaces carried out in an ultrahigh-vacuum. Their calculations performed on Cu(111) and Cu nanoparticles unsupported and deposited on ZnO(0001) indicated that methanol production via the RWGS pathway is hindered by the first hydrogenation of CO to HCO. The latter is not stable on Cu and prefers to dissociate into CO and H. Therefore, the faster RWGS only leads to the accumulation of CO, rather the methanol formation.

Results obtained by microkinetic modelling, dimer method and combination of theoretical and experimental studies show that the use of different methods for examination of reaction pathways can lead to completely opposite conclusions. Similarly, Zhang et al.[174] studied optimum Cu nanoparticles for CO_2 hydrogenation towards methanol synthesis with DFT and PBE functional and microkinetic modelling following the elementary reaction steps depicted in figure 11b. This mechanism involves direct CO_2 dissociation to CO and O and generation of HCO intermediate. The comparison of CO_2 adsorption was made between different types of Cu clusters (Cu13, Cu15, Cu19, Cu55, Cu99) and Cu(111) and Cu(211) surfaces shown in figure 11a. They reported that intermediate sized Cu19

clusters are optimal for CO_2 hydrogenation and the Cu particle size effect originates from changes in the adsorption energies of the reaction intermediates which can be correlated to the location of the d-band of the Cu clusters that strengthens the bonding interaction between metal and intermediates and therefore influencing CO_2 reduction activity. However, their results are in stark contrast with experimental results of Berg et al.[206] where they studied the catalytic activity of reduced Cu(Zn)/C catalysts obtained from Cu(Zn)/SiO_2 and Cu/ZnO(/Al_2O_3) samples using synthesis gas composed of 10% Ar, 7% CO_2, 23% CO and 60% H_2 . It was shown that particles smaller than ~8 nm are less active than larger particles per surface area of copper. The difference between theoretical and experimental data may be the result of the conditions that are more industrially correct for experimental studies. While simulations consider only the CO_2 molecule the experiment works with a synthesis gas which has certain ratio of various gases that can affect the results of nanocatalyst's activity.

Figure 11 a) The Adsorption energy and favourable adsorption structures of CO_2 and H on Cu_{19} and Cu(111) and Cu(211) surfaces c) CO_2 hydrogenation to methanol on Cu extended surfaces.[174]

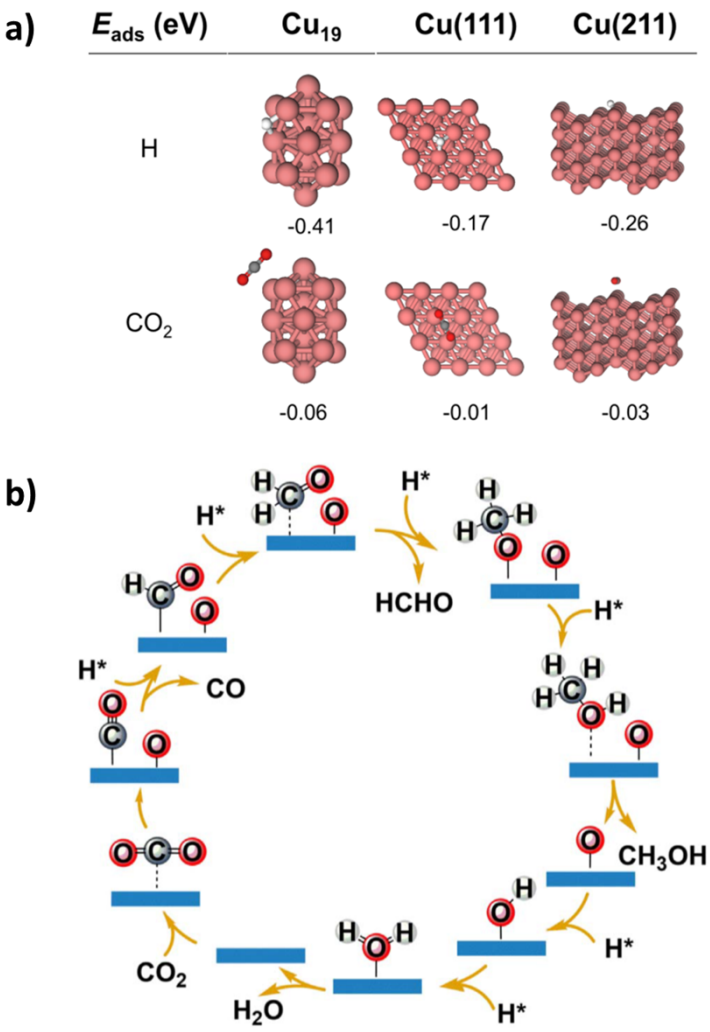

Some researchers included Zn into the Cu surface to study the effect of CuZn catalysts on CO_2 hydrogenation. Behrens et al.[207] performed DFT calculations of CO_2 hydrogenation to methanol on Cu(111), Cu(211) surfaces and CuZn(211) where Cu in the step was partially substituted by Zn. According to their results hydrogenation of CO_2 proceeded via formate mechanism (formation of HCOO, HCOOH and H_2COOH), although the formate intermediate was identified as spectator species bypreviously mentioned articles. Cu(111) surface bounded the intermediates more weakly than

Cu(211) and alloying of Zn into the Cu step increased the adsorption strength of intermediates and decreased barriers. If more Zn atoms are considered in the CuZn(211) surface, the binding to these species is further strengthened. Therefore, the presence of steps and Zn is required for higher activity towards methanol.
In summary, theoretical studies show different results and are not uniform in identifying the reaction pathway for methanol synthesis on copper surface.

3.3.4 Rh catalytic surfaces

In methanol synthesis: Rh metal surfaces are poorly examined by computational studies and there is no DFT study on pure Rh surfaces. Recently, Liu et al.[208] explored the effect of Rh doped Cu(111) surfaces (Cu(111), Rh_3Cu_6(111), Rh_6Cu_3(111) and Rh ML surfaces) on CO_2 hydrogenation via RWGS pathway using GGA with PW91 functional together with DNP function. The calculated results shown both kinetic and thermodynamic facilitation of methanol synthesis, especially on Rh_3Cu_6(111) surface. The most intermediates adsorbing through C atom preferred to bind at the Rh site and were strengthened by the doped Rh. The rate-limiting steps were CO_2 hydrogenation to trans-COOH* on Cu(111) and Rh_3Cu_6(111) surfaces, and the formation of HCO* from CO* hydrogenation on Rh_6Cu_3(111) and Rh ML surfaces. Furthermore, the by-product of CO was inhibited due to the dissociative adsorption of H_2.

3.2.5 Pd catalytic surfaces

Similarly, as with Rh surfaces the Pd metal surfaces are not well investigated by DFT methods. Only few studies deal with computational calculations and describe the mechanism of CO_2 hydrogenation on Pd surfaces.
In methanol synthesis: Zhang et al.[209] proposed a mechanism of methanol synthesis from CO_2 hydrogenation on Pd(111) surface using GGA approximation with PBE functional. They suggested that CO_2 can be chemically adsorbed as a bidentate configuration on Pd(111) hollow site consisting of three Pd atoms and the H_2 can dissociate to H atoms spontaneously. The lower adsorption energy -0.70 eV indicated that the CO_2 can be activated by Pd, however the adsorption is weak. This shows that Pd catalyst would be a better catalyst in combination with other metal or chemical compound. The adsorption configuration of CO_2 and H atoms is presented in Figure 12a). The HCOO and COOH intermediates are both possible to form via the reaction between the CO_2 and the surface H atom which is displayed on Figure 12b). By further hydrogenation of HCOO or HCOOH intermediate HCOOH is generated. In the next step HCOOH dissociates to HCO, which then hydrogenates consecutively to H_2CO, H_3CO and H_3COH ultimately. In their study, the formation of H_2CO is the rate-limiting step with an activation barrier of 0.91 eV and CO is the by-product, formed mainly from the dissociation of COOH. Two reaction pathways are depicted in Figure 12.
Liu et al.[210] using GGA with PW91 functional together with DNP function found out that the addition of Pd atoms on the Cu(111) surface not only affect the adsorption configuration but also alter the interactions between the adsorbed species and the metal surfaces. The rate-limiting step was the formation of trans-COOH* from CO_2 hydrogenation on Pd_3Cu_6(111) and Pd_6Cu_3(111) surfaces which is the same as on pure Cu(111) surface, however, it changed to cis-COOH* decomposition to CO* and OH* on Pd ML surface. The change of the rate-limiting step was mainly due to the strengthened adsorption of COOH*, while the adsorption of OH* was greatly weakened by the added monolayer of Pd atoms.

Figure 12 a) The adsorption configuration of CO_2 and H atoms on the Pd(111) surface, b) HCOO reaction route of CO_2 hydrogenation and c) COOH reaction route of CO_2 hydrogenation [reprinted by permission from[211], Copyright 2019].

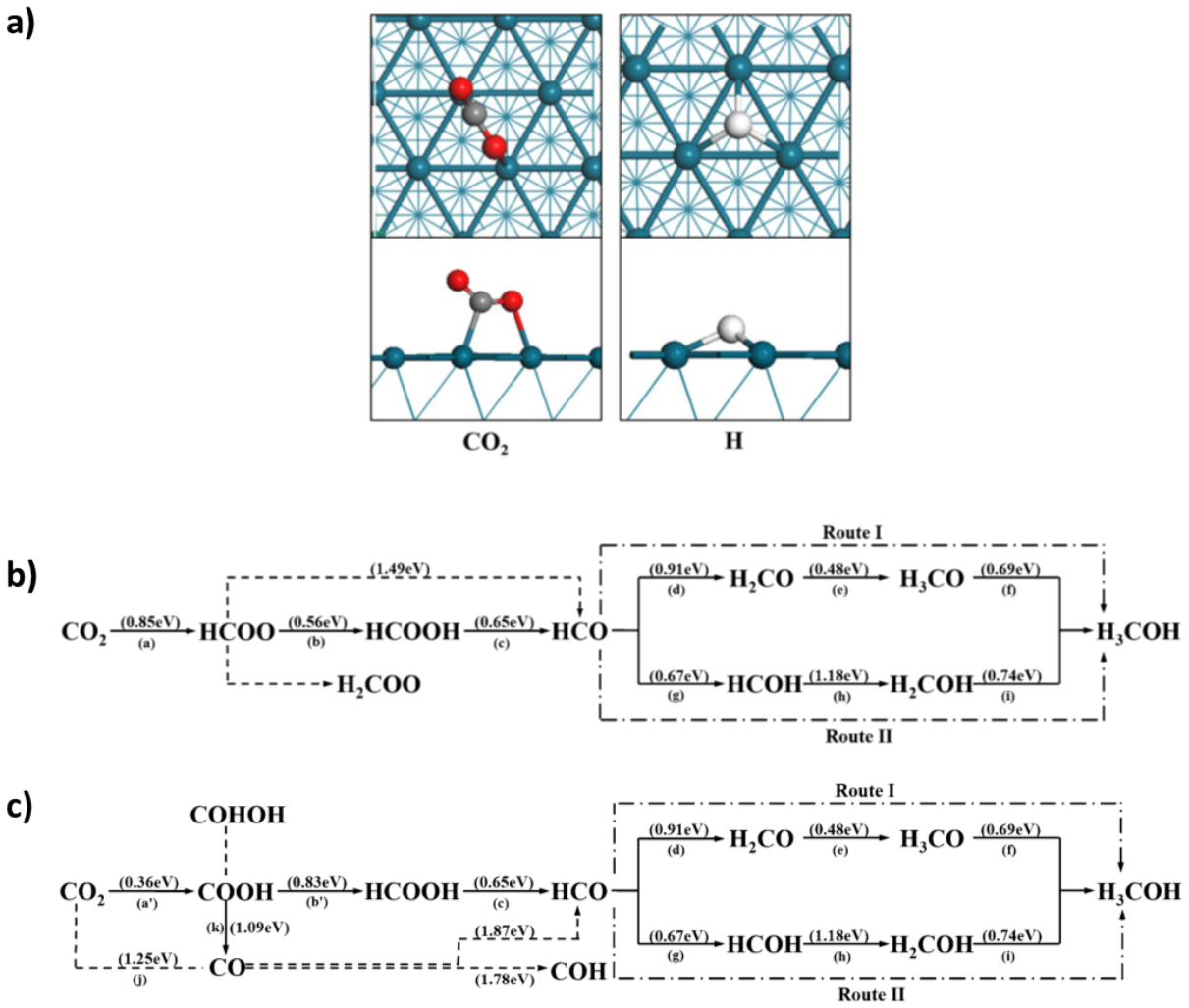

Pd(111) surface was examined in combination with Cu(111) by Jiang et al.[212] using PAW potentials and spin-polarized GGA with PBE functional and catalytic tests of Pd-Cu bimetallic catalysts in fixed-bed reactor. Pd-Cu bimetallic combination enhanced the adsorption of H_2 and CO_2, although, the adsorption strength was still weak. DFT results shown formation of HCOO* intermediate. In the transition state configuration for HCOO* formation, the two O atoms of bent CO_2 are stabilized by two Pd atoms on the surface; the H* atom bonds to the remaining Pd atom in the triangle site and attacks the C atom of CO_2 for hydrogenation.

These studies have shown that the adsorption of CO_2 on the Pd surfaces is weak. However, the microkinetic studies could bring more light to the mechanism of CO_2 hydrogenation on Pd surfaces. Therefore, finding a right combination of Pd catalyst with different type of catalyst is needed to increase the CO_2 adsorption and more DFT calculations in this direction are needed.

4. Conclusions

The DFT simulations of CO_2 on transition metal surfaces provide information about the intricate mechanisms of CO_2 hydrogenation. Understanding of elementary processes on atomic scale is important to design novel catalysts with outstanding activity and selectivity towards specific compounds. Here, a review of the current understanding of CO_2 catalytic hydrogenation to fuels and chemicals including CO, CH_4, CH_3OH and HCOOH and mechanisms with different reaction pathways and elementary steps is presented.

Our review shows that surface and adsorption energies values are highly affected using different functional. Several studies displayed that the best results of adsorption energies for transition metals can be currently provided by BEEF-vdW, M06-L, GAM functionals and RPA method. Recent DFT calculations provides interesting insights into the adsorption, dissociation of CO_2 and overall reaction mechanism of CO_2 hydrogenation on different transition metal surfaces, however many studies do not include the microkinetic modelling which could provide more information about the mechanisms and intermediates. Moreover, as it was mentioned with Cu-based catalysts, several DFT studies in combination with microkinetic modelling present opposite results not only in comparison to experimental data but also in comparison with each other.

Current research should be focused not only on the comparison of various facets of transition metals but also on the different type of metal structures which can change a catalytic effect and help to better control the whole CO_2 hydrogenation process. Seeing that metals such as Rh, Pt, Au, Ag are expensive for experimental research, more computational simulations of these surface would be financially advantageous. DFT simulations would also be very useful in CO_2 conversion to formic acid since the synthesis of catalysts is complicated and very energy consuming. There are not many studies that deal with catalyst development for formic acid synthesis which has after methane the second largest storing capacity for hydrogen.

In conclusion, CO_2 hydrogenation is still not completely understood and controlled. DFT studies are a great tool to help understanding individual steps of the reaction. Many options and questions can be investigated and discussed by computational approach and contribute to obtain superior catalysts which would make the whole process more effective and selective towards specific chemicals.

Acknowledgements

This work was supported by the Scientific Grant Agency of the Ministry of Education, Science, Research, and Sport of the Slovak Republic project no. VEGA 1/0074/17. VS gratefully acknowledges the Generalitat Valenciana (CIDEGENT/2018/036) for funding.

Keywords: CO_2, DFT, heterogeneous catalysis, hydrogenation, transition metals

References

[1] D. J. Wuebbles, D. W. Fahey, K. A. Hibbard, *Climate Science Special Report: Fourth National Climate Assessment*, **2017**.

[2] V. Masson-Delmotte, P. Zhai, H.-O. Pörtner, D. Roberts, J. Skea, P.R., P. R. Shukla, A. Pirani, W. Moufouma-Okia, C. Péan, et al., *Global Warming of 1.5°C: An IPCC Special Report on the Impacts of Global Warming of 1.5°C above Pre-Industrial Levels and Related Global Greenhouse Gas Emission Pathways, in the Context of Strengthening the Global Response to the Threat of Climate Change,* **2018**.

[3] S. Kar, J. Kothandaraman, A. Goeppert, G. K. S. Prakash, *J. CO2 Util.* **2018**, *23*, 212–218.

[4] M. A. Scibioh, B. Viswanathan, *Homogeneous Hydrogenation of CO2*, **2018**.

[5] S. Dang, H. Yang, P. Gao, H. Wang, X. Li, W. Wei, Y. Sun, *Catal. Today* **2019**, *330*, 61–75.

[6] M. A. Scibioh, B. Viswanathan, *Heterogeneous Hydrogenation of CO2*, **2018**.

[7] M. A. Scibioh, B. Viswanathan, *Biochemical Reduction of CO2*, **2018**.
[8] C. Chen, J. F. Khosrowabadi Kotyk, S. W. Sheehan, *Chem* **2018**, *4*, 2571–2586.
[9] F. Zhang, H. Zhang, Z. Liu, *Curr. Opin. Green Sustain. Chem.* **2019**, *16*, 77–84.
[10] O. G. Sánchez, Y. Y. Birdja, M. Bulut, J. Vaes, T. Breugelmans, D. Pant, *Curr. Opin. Green Sustain. Chem.* **2019**, *16*, 47–56.
[11] A. A. Khan, M. Tahir, *J. CO2 Util.* **2019**, *29*, 205–239.
[12] M. A. Scibioh, B. Viswanathan, *Carbon Dioxide to Chem. Fuels* **2018**, *3*, 109–126.
[13] Y. Wang, D. He, H. Chen, D. Wang, *J. Photochem. Photobiol. C Photochem. Rev.* **2019**, *40*, 117.
[14] M. Aresta, A. Dibenedetto, E. Quaranta, *J. Catal.* **2016**, *343*, 2–45.
[15] A. Álvarez, M. Borges, J. J. Corral-Pérez, J. G. Olcina, L. Hu, D. Cornu, R. Huang, D. Stoian, A. Urakawa, *ChemPhysChem* **2017**, *18*, 3135–3141.
[16] E. V. Kondratenko, G. Mul, J. Baltrusaitis, G. O. Larrazábal, J. Pérez-Ramírez, *Energy Environ. Sci.* **2013**, *6*, 3112–3135.
[17] H. S. Whang, J. Lim, M. S. Choi, J. Lee, H. Lee, *BMC Chem. Eng.* **2019**, *1*, 9.
[18] M. Liu, Y. Yi, L. Wang, H. Guo, A. Bogaerts, *Catalysts* **2019**, *9*, 275.
[19] W. Li, H. Wang, X. Jiang, J. Zhu, Z. Liu, X. Guo, *RSC Advaces* **2018**, 7651–7669.
[20] H. Yang, C. Zhang, P. Gao, W. Hui, X. Li, L. Zhong, W. Wei, Y. Sun, *Catal. Sci. Technol.* **2017**, *7*, 4580–4598.
[21] Y. Li, S. H. Chan, Q. Sun, *Nanoscale* **2015**, *7*, 8663–8683.
[22] L. C. Grabow, M. Mavrikakis, *ACS Catal.* **2011**, *1*, 365–384.
[23] O. Tursunov, L. Kustov, A. Kustov, *Oil Gas Sci. Technol.* **2017**, *72*, 30.
[24] M. R. Gogate, *Pet. Sci. Technol.* **2019**, *37*, 603–610.
[25] Y. Liu, J. Liu, S. Liu, J. Li, Z. Gao, Z. Zuo, *J. CO2 Util.* **2017**, *20*, 59–65.
[26] R. M. Palomino, P. J. Ramírez, Z. Liu, R. Hamlyn, I. Waluyo, M. Mahapatra, I. Orozco, A. Hunt, J. P. Simonovis, S. D. Senanayake, et al., *J. Phys. Chem. B* **2018**, *122*, 794–800.
[27] D. Cheng, F. R. Negreiros, E. Aprà, A. Fortunelli, *ChemSusChem* **2013**, *6*, 944–965.
[28] D. Weijing, Z. Weihong, Z. Xiaodong, Z. Baofeng, C. Lei, S. Laizhi, Y. Shuangxia, G. Haibin, C. Guanyi, Z. Liang, et al., *Energy Procedia* **2018**, *152*, 997–1002.
[29] X. Jiang, X. Wang, X. Nie, N. Koizumi, X. Guo, C. Song, *Catal. Today* **2018**, *316*, 62–70.
[30] W. D. Shafer, G. Jacobs, U. M. Graham, H. H. Hamdeh, B. H. Davis, *J. Catal.* **2019**, *369*, 239–248.
[31] B. C. Sempuga, Y. Yao, *J. CO2 Util.* **2017**, *20*, 34–42.
[32] S. Saeidi, N. A. S. Amin, M. R. Rahimpour, *J. CO2 Util.* **2014**, *5*, 66–81.
[33] J. Gao, C. Jia, B. Liu, *Catal. Sci. Technol.* **2017**, *7*, 5602.
[34] G. Peng, S. J. Sibener, G. C. Schatz, M. Mavrikakis, *Surf. Sci.* **2012**, *606*, 1050–1055.
[35] C. S. He, L. Gong, J. Zhang, P. P. He, Y. Mu, *J. CO2 Util.* **2017**, *19*, 157–164.
[36] C. L. Chiang, K. S. Lin, H. W. Chuang, *J. Clean. Prod.* **2018**, *172*, 1957–1977.
[37] J. Sirijaraensre, J. Limtrakul, *Appl. Surf. Sci.* **2016**, *364*, 241–248.
[38] Y. A. Daza, J. N. Kuhn, *RSC Adv.* **2016**, *6*, 49675–49691.
[39] I. Kuznecova, J. Gusca, *Energy Procedia* **2017**, *128*, 255–260.
[40] X. Su, J. Xu, B. Liang, H. Duan, B. Hou, Y. Huang, *J. Energy Chem.* **2016**, *25*, 553–565.
[41] S. A. Al-Saydeh, S. J. Zaidi, *Carbon Dioxide Conversion to Methanol: Opportunities and Fundamental Challenges*, **2018**.
[42] O. A. Ojelade, S. F. Zaman, *Catal. Surv. from Asia* **2019**, DOI 10.1007/s10563-019-09287-z.
[43] B. Yan, B. Zhao, S. Kattel, Q. Wu, S. Yao, D. Su, J. G. Chen, *J. Catal.* **2019**, *374*, 60–71.
[44] J. A. Rodriguez, P. Liu, D. J. Stacchiola, S. D. Senanayake, M. G. White, J. G. Chen, *ACS Catal.* **2015**, *5*, 6696–6706.
[45] A. Lähdetie, P. Nousiainen, A. Jääskeläinen, *Chem. Commun.* **2015**, *51*, 6988.
[46] M. D. Porosoff, X. Yang, J. A. Boscoboinik, J. G. Chen, *Angew. Chemie - Int. Ed.* **2014**, *53*, 6705–6709.
[47] S. Liu, H. Zhou, Q. Song, Z. Ma, *J. Taiwan Inst. Chem. Eng.* **2017**, *76*, 18–26.
[48] C. Liu, P. Liu, *ACS Catal.* **2015**, *5*, 1004–1012.
[49] D. V. Leybo, N. I. Kosova, K. O. Chuprunov, D. V. Kuznetsov, I. A. Kurzina, *Adv. Mater. Res.* **2014**, *872*, 3–9.
[50] Y. Ma, G. Guan, X. Hao, J. Cao, A. Abudula, *Renew. Sustain. Energy Rev.* **2017**, *75*, 1101–

1129.
[51] A. B. Dongil, *Nanomaterials* **2019**, *9*, DOI 10.3390/nano9081111.
[52] A. K. Mishra, A. Roldan, N. H. De Leeuw, *J. Phys. Chem. C* **2016**, *120*, 2198–2214.
[53] Q. Tang, Q. Luo, *J. Phys. Chem. C* **2013**, *117*, 22954–22966.
[54] W. G. Reimers, M. A. Baltanás, *J. Mol. Model.* **2014**, *20*, 2270.
[55] M. Dou, M. Zhang, Y. Chen, *New J. Chem.* **2018**, *42*, 3293–3300.
[56] L. Wang, T. Maxisch, G. Ceder, *Phys. Rev. B* **2006**, *73*, 1–6.
[57] B. Hu, C. Guild, S. L. Suib, *J. CO2 Util.* **2013**, *1*, 18–27.
[58] Q. Liu, L. Wu, R. Jackstell, M. Beller, *Nat. Commun.* **2015**, *6*, 1–15.
[59] L. Wang, W. Sun, C. Liu, *Chinese J. Chem.* **2018**, *36*, 353–362.
[60] W. Benzinger, E. Daymo, M. Hettel, L. Maier, C. Antinori, P. Pfeifer, O. Deutschmann, *Chem. Eng. J.* **2019**, *362*, 430–441.
[61] C. Graves, S. D. Ebbesen, M. Mogensen, K. S. Lackner, *Renew. Sustain. Energy Rev.* **2011**, *15*, 1–23.
[62] X. Su, X. Yang, B. Zhao, Y. Huang, *J. Energy Chem.* **2017**, *26*, 854–867.
[63] R. J. Byron Smith, L. Murugananda, S. Murthy Shekhar, *Int. J. Chem. React. Eng.* **2010**, *8*.
[64] S. Saeidi, S. Najari, F. Fazlollahi, M. K. Nikoo, F. Sefidkon, J. J. Klemeš, L. L. Baxter, *Renew. Sustain. Energy Rev.* **2017**, *80*, 1292–1311.
[65] X. Yan, H. Guo, D. Yang, S. Qiu, X. Yao, *Curr. Org. Chem.* **2014**, *18*, 1335–1345.
[66] M. Aresta, A. Dibenedetto, E. Quaranta, *Reaction Mechanisms in Carbon Dioxide Conversion*, **2015**.
[67] C.-S. Chen, W.-H. Cheng, S. Lin, *Catal. Letters* **2000**, *68*, 45–48.
[68] N. Homs, J. Toyir, P. R. De La Piscina, *Catalytic Processes for Activation of CO2*, Elsevier B.V., **2014**.
[69] R. J. Byron Smith, L. Murugananda, S. Murthy Shekhar, *Int. J. Chem. React. Eng.* **2010**, *8*.
[70] D. L. Jurković, A. Pohar, V. D. B. C. Dasireddy, B. Likozar, *Chem. Eng. Technol.* **2017**, *40*, 973–980.
[71] C. Álvarez Galván, J. Schumann, M. Behrens, J. L. G. Fierro, R. Schlögl, E. Frei, *Appl. Catal. B Environ.* **2016**, *195*, 104–111.
[72] S. S. Kim, H. H. Lee, S. C. Hong, *"Applied Catal. A, Gen.* **2012**, *423–424*, 100–107.
[73] G. Pekridis, K. Kalimeri, N. Kaklidis, E. Vakouftsi, E. F. Iliopoulou, *Catal. Today* **2007**, *127*, 337–346.
[74] H. Karadeniz, C. Karakaya, S. Tischer, O. Deutschmann, *Zeitschrift für Phys. Chemie* **2015**, *229*, DOI 10.1515/zpch-2014-0622.
[75] L. Pastor-Pérez, F. Baibars, E. Le Sache, H. Arellano-García, S. Gu, T. R. Reina, *J. CO2 Util.* **2017**, *21*, 423–428.
[76] Amit A. Gokhale, James A. Dumesic, and Manos Mavrikakis, *J. Am. Chem. Soc.* **2008**, *130*, 1402–1414.
[77] G. Zhou, B. Dai, H. Xie, G. Zhang, K. Xiong, X. Zheng, *J. CO2 Util.* **2017**, *21*, 292–301.
[78] X. Zhang, X. Zhu, L. Lin, S. Yao, M. Zhang, X. Liu, X. Wang, Y. Li, C. Shi, *ACS Catal.* **2017**, *7*, 912–918.
[79] H. Xu, X. Luo, J. Wang, Y. Su, X. Zhao, Y. Li, *ACS Appl. Mater. Interfaces* **2019**, *11*, 20291–20297.
[80] A. G. Kharaji, A. Shariati, M. Ostadi, *J. Nanosci. Nanotechnol.* **2014**, *14*, 6841–6847.
[81] M. I. Qadir, F. Bernardi, J. D. Scholten, D. L. Baptista, *Appl. Catal. B Environ.* **2019**, *252*, 10–17.
[82] L. Wang, H. Liu, Y. Chen, S. Yang, *Int. J. Hydrogen Energy* **2016**, *42*, 3682–3689.
[83] Y. Shen, Z. Cao, Z. Xiao, *Catalysts* **2019**, *9*, 423.
[84] L. Pastor-Pérez, M. Shah, *Catalysts* **2018**, *8*, 608.
[85] D. L. Williamson, C. Herdes, L. Torrente-murciano, M. D. Jones, D. Mattia, *ACS Sustain. Chem. Eng.* **2019**, *7*, 7395–7402.
[86] X. Zhang, X. Zhu, L. Lin, S. Yao, M. Zhang, X. Liu, X. Wang, *ACS Catal.* **2017**, *7*, 912–918.
[87] H. Jing, L. Iaohong, J. Wang, D. Liu, K. Wu, *J. Phys. Chem. C* **2018**, *123*, 1235–1251.
[88] A. Wolf, A. J. Jess, C. K. Kern, *Chem. Eng. Technol.* **2016**, *39*, 1040–1048.
[89] X. Chen, X. Su, H. Duan, B. Liang, Y. Huang, *Catal. Today* **2017**, *281*, 312–318.
[90] S. Kattel, B. Yan, J. G. Chen, P. Liu, *J. Catal.* **2016**, *343*, 115–126.
[91] X. Chen, X. Su, H. Duan, B. Liang, Y. Huang, *Catal. Today* **2017**, *281*, 312–318.

[92] S. M. Lee, H. Eom, S. S. Kim, *Environ. Technol.* **2019**, *3330*, 1–27.
[93] S. Choi, B. I. Sang, J. Hong, K. J. Yoon, J. W. Son, J. H. Lee, B. K. Kim, H. Kim, *Sci. Rep.* **2017**, *7*, 1–10.
[94] L. Yang, L. Pastor-Pérez, S. Gu, A. Sepúlveda-Escribano, T. R. Reina, **2018**, *232*, 464–471.
[95] W. Wang, J. Gong, *Front. Chem. Eng. China* **2011**, *5*, 2–10.
[96] B. Miao, S. S. K. Ma, X. Wang, H. Su, S. H. Chan, *Catal. Sci. Technol.* **2016**, *6*, 4048–4058.
[97] Z. Qin, Y. Zhou, Y. Jiang, Z. Liu, H. Ji, *Intech open* **2018**, *2*, 64.
[98] Y. A. Agafonov, L. A. Tishkova, A. L. Lapidus, T. N. Myshenkova, N. A. Gaidai, N. V. Nekrasov, *Pet. Chem.* **2007**, *47*, 75–82.
[99] S. Tada, R. Kikuchi, *Catal. Sci. Technol.* **2015**, 3061–3070.
[100] M. Mihet, O. Grad, G. Blanita, T. Radu, M. D. Lazar, *Int. J. Hydrogen Energy* **2019**, *44*, 13383–13396.
[101] B. Alrafei, I. Polaert, A. Ledoux, F. Azzolina-Jury, *Catal. Today* **2019**, DOI 10.1016/j.cattod.2019.03.026.
[102] D. Zhong, L. Ouyang, J. Liu, H. Wang, Y. Jia, M. Zhu, *Int. J. Hydrogen Energy* **2019**, *44*, 29068.
[103] A. Porta, L. Falbo, C. G. Visconti, L. Lietti, C. Bassano, P. Deiana, *Catal. Today* **2019**, 0–1.
[104] S. Navarro-Jaén, J. C. Navarro, L. F. Bobadilla, M. A. Centeno, O. H. Laguna, J. A. Odriozola, *Appl. Surf. Sci.* **2019**, *483*, 750–761.
[105] H. T. T. Nguyen, Y. Kumabe, S. Ueda, K. Kan, M. Ohtani, K. Kobiro, *Appl. Catal. A Gen.* **2019**, *577*, 35–43.
[106] I. V. Yentekakis, G. Goula, M. Hatzisymeon, I. Betsi-Argyropoulou, G. Botzolaki, K. Kousi, D. I. Kondarides, M. J. Taylor, C. M. A. Parlett, A. Osatiashtiani, et al., *Appl. Catal. B Environ.* **2019**, *243*, 490–501.
[107] A. Karelovic, P. Ruiz, *J. Catal.* **2013**, *301*, 141–153.
[108] H. Jiang, Q. Gao, S. Wang, Y. Chen, M. Zhang, *J. CO_2 Util.* **2019**, *31*, 167–172.
[109] J. N. Park, E. W. McFarland, *J. Catal.* **2009**, *266*, 92–97.
[110] W. Li, Y. Liu, M. Mu, F. Ding, Z. Liu, X. Guo, C. Song, *"Applied Catal. B, Environ.* **2019**, *254*, 531.
[111] W. Li, X. Nie, X. Jiang, A. Zhang, F. Ding, M. Liu, Z. Liu, *Appl. Catal. B Environ.* **2018**, *220*, 397–408.
[112] T. Burger, F. Koschany, O. Thomys, K. Köhler, O. Hinrichsen, *Appl. Catal. A, Gen.* **2018**, *558*, 44–54.
[113] D. Pandey, K. Ray, R. Bhardwaj, S. Bojja, K. V. R. Chary, G. Deo, *Int. J. Hydrogen Energy* **2018**, *43*, 4987–5000.
[114] A. H. Zamani, N. Akmar, M. Shohaimi, S. Jamal, M. Rosid, N. Hakimin, N. Mohd, *J. Taiwan Inst. Chem. Eng.* **2019**, *96*, 400–408.
[115] P. Dumrongbunditkul, T. Witoon, M. Chareonpanich, *Ceram. Int.* **2016**, *42*, 10444–10451.
[116] M. Mihet, M. D. Lazar, *Catal. Today* **2018**, *306*, 294–299.
[117] J. Gao, Q. Liu, F. Gu, B. Liu, Z. Zhong, F. Su, *RSC Adv.* **2015**, *5*, 22759–22776.
[118] M. Younas, L. L. Kong, M. J. K. Bashir, H. Nadeem, A. Shehzad, S. Sethupathi, *Energy Fuels* **2016**, *30*, 8815–8831.
[119] T. Sakpal, L. Lefferts, *J. Catal.* **2018**, *367*, 171–180.
[120] X. Ding, L. De Rogatis, E. Vesselli, A. Baraldi, G. Comelli, R. Rosei, L. Savio, L. Vattuone, M. Rocca, P. Fornasiero, et al., *Phys. Rev. B - Condens. Matter Mater. Phys.* **2007**, *76*, 1–12.
[121] C. Mebrahtu, F. Krebs, S. Abate, S. Perathoner, G. Centi, R. Palkovits, in *Horizons Sustain. Ind. Chem. Catal.*, Elsevier B.V., **2019**, pp. 85–103.
[122] J. Gao, Q. Liu, F. Gu, B. Liu, Z. Zhong, F. Su, *RSC Adv.* **2015**, *5*, 22759–22776.
[123] E. S. Gnanakumar, N. Chandran, I. V Kozhevnikov, A. Grau-atienza, E. V Ramos, A. Sepulveda-escribano, N. R. Shiju, *Chem. Eng. Sci.* **2019**, *194*, 2–9.
[124] R. Daroughegi, F. Meshkani, M. Rezaei, *J. Energy Inst.* **2019**, 1–14.
[125] G. Garbarino, C. Wang, T. Cavattoni, E. Finocchio, P. Riani, M. Flytzani-stephanopoulos, G. Busca, *Appl. Catal. B Environ.* **2019**, *248*, 286–297.
[126] Z. Li, T. Zhao, L. Zhang, *Appl. Organomet. Chem.* **2018**, *32*, 1–7.
[127] L. Zhou, L. R. Enakonda, M. Harb, Y. Saih, A. Aguilar-Tapia, S. Ould-Chikh, J. louis Hazemann, J. Li, N. Wei, D. Gary, et al., *Appl. Catal. B Environ.* **2017**, *208*, 44–59.
[128] D. Tian, Z. Liu, D. Li, H. Shi, W. Pan, Y. Cheng, *Fuel* **2013**, *104*, 224–229.

[129] S. Hwang, U. G. Hong, J. Lee, J. G. Seo, J. H. Baik, D. J. Koh, H. Lim, I. K. Song, *J. Ind. Eng. Chem.* **2013**, *19*, 2016–2021.
[130] A. S. Sandupatla, A. Banerjee, G. Deo, *Appl. Surf. Sci.* **2019**, *485*, 441.
[131] R. R. C. M. Silva, H. A. Oliveira, A. C. P. F. Guarino, T. M. Oliveira, B. B. Toledo, M. B. T. Moura, F. B. Passos, *Int. J. Hydrogen Energy* **2016**, *41*, 6763–6772.
[132] C. Huang, J. Wen, Y. Sun, M. Zhang, Y. Bao, *Chem. Eng. J.* **2019**, *374*, 221–230.
[133] G. Leonzio, E. Zondervan, P. Ugo, *Int. J. Hydrogen Energy* **2019**, *44*, 7915–7933.
[134] H. L. Fang, J. Cole, Z. Wu, M. Qin, Z. He, *J. Adv. Nanomater.* **2017**, *2*, 1–10.
[135] M. Qiu, H. Tao, R. Li, Y. Li, X. Huang, W. Chen, W. Su, *J. Chem. Phys.* **2016**, *134701*, DOI 10.1063/1.4963384.
[136] Y. Yang, C. A. Mims, R. S. Disselkamp, J. H. Kwak, C. H. F. Peden, C. T. Campbell, *J. Phys. Chem. C* **2010**, *114*, 17205–17211.
[137] Q. L. Tang, Q. J. Hong, Z. P. Liu, *J. Catal.* **2009**, *263*, 114–122.
[138] P. A. Taylor, P. B. Rasmussen, I. Chorkendorff, *J. Chem. Soc. Faraday Trans.* **1995**, *91*, 1267–1269.
[139] M. Behrens, O. Access, *Recycl. Catal.* **2015**, *2*, 78–86.
[140] Y. Chen, H. Li, W. Zhao, W. Zhang, J. Li, W. Li, X. Zheng, W. Yan, W. Zhang, J. Zhu, et al., *Nat. Commun.* **2019**, *10*, 1–8.
[141] D. Allam, S. Bennici, L. Limousy, S. Hocine, *Comptes rendus - Chim.* **2019**, *22*, 227–237.
[142] S. Li, Y. Wang, B. Yang, L. Guo, *Appl. Catal. A, Gen.* **2019**, *571*, 51–60.
[143] M. S. Tameh, A. K. Dearden, C. Huang, *J. Phys. Chem. C* **2018**, *122*, 17942–17953.
[144] J. Nakamura, I. Nakamura, T. Uchijima, T. Watanabe, T. Fujitani, *Stud. Surf. Sci. Catal.* **1996**, *101 B*, 1389–1399.
[145] S. Kuld, M. Thorhauge, H. Falsig, C. F. Elkjær, S. Helveg, I. Chorkendorff, J. Sehested, *Science (80-.).* **2016**, *352*, 969–974.
[146] M. Behrens, F. Studt, I. Kasatkin, S. Kühl, M. Hävecker, F. Abild-Pedersen, S. Zander, F. Girgsdies, P. Kurr, B. L. Kniep, et al., *Science (80-.).* **2012**, *336*, 893–897.
[147] F. Studt, M. Behrens, E. L. Kunkes, N. Thomas, S. Zander, A. Tarasov, J. Schumann, E. Frei, J. B. Varley, F. Abild-Pedersen, et al., *ChemCatChem* **2015**, *7*, 1105–1111.
[148] M. Bowker, *ChemCatChem* **2019**, *11*, 4238–4246.
[149] A. Weilhard, M. I. Qadir, V. Sans, J. Dupont, *ACS Catal.* **2018**, *8*, 1628–1634.
[150] T. Schaub, *Phys. Sci. Rev.* **2018**, *3*, 1–14.
[151] M. D. Esra, B. Nejadebrahimi, *Appl. Surf. Sci.* **2019**, *475*, 363–371.
[152] H. Reymond, J. J. Corral-Pérez, A. Urakawa, P. Rudolf von Rohr, *React. Chem. Eng.* **2018**, *3*, 912–919.
[153] W. Zhang, S. Wang, Y. Zhao, X. Ma, *Fuel Process. Technol.* **2018**, *178*, 98–103.
[154] G. A. Filonenko, W. L. Vrijburg, E. J. M. Hensen, E. A. Pidko, *J. Catal.* **2016**, *343*, 97–105.
[155] D. Preti, C. Resta, S. Squarcialupi, G. Fachinetti, *Angew. Chemie - Int. Ed.* **2011**, *123*, 12759–12762.
[156] P. Upadhyay, V. Srivastava, *Present Environ. Sustain. Dev.* **2016**, *10*, 13–34.
[157] K. Rohmann, J. Kothe, M. W. Haenel, U. Englert, M. Hçlscher, *Angew. Chemie - Int. Ed.* **2016**, *55*, 8966–8969.
[158] S. Moret, P. J. Dyson, G. Laurenczy, *Nat. Commun.* **2014**, *5*, 1–7.
[159] H. Lo, C. Copéret, *ChemCatChem* **2019**, *9*, 430–434.
[160] J. Fidalgo, M. Ruiz-Castaneda, G. García-Herbosa, A. Carbayo, F. A. Jalón, A. M. Rodríguez, B. R. Manzano, G. Espino, *Inorg. Chem.* **2018**, *57*, 14186–14198.
[161] P. Gautam, P. Ramprakash, U. Vivek, *Catal. Letters* **2019**, *149*, 1464–1475.
[162] H. Lo, I. Thiel, C. Copéret, *Chem. - A Eur. J.* **2019**, *25*, 9443–9446.
[163] Z. Zhang, L. Zhang, S. Yao, X. Song, W. Huang, M. J. Hülsey, *J. Catal.* **2019**, *376*, 57–67.
[164] W. Wang, Y. Himeda, J. T. Muckerman, G. F. Manbeck, E. Fujita, *Chem. Rev.* **2015**, *115*, 12936–12973.
[165] N. Onishi, S. Xu, Y. Manaka, Y. Suna, W.-H. Wang, J. T. Muckerman, E. Fujita, Y. Himeda, *Inorg. Chem.* **2015**, *54*, 5114–5123.
[166] Y. M. Badiei, W.-H. Wang, J. F. Hull, D. J. Szalda, J. T. Muckerman, Y. Himeda, E. Fujita, *Inorg. Chem.* **2013**, *52*, 12576–12586.
[167] L. Dietz, S. Piccinin, M. Maestri, *J. Phys. Chem. C* **2015**, *119*, 4959.

[168] J. P. Clay, J. P. Greeley, F. H. Ribeiro, W. N. Delgass, W. F. Schneider, *J. Catal.* **2014**, *320*, 106–117.
[169] T. Nilsson Pingel, M. Jørgensen, A. B. Yankovich, H. Grönbeck, E. Olsson, *Nat. Commun.* **2018**, *9*, DOI 10.1038/s41467-018-05055-1.
[170] M. Escudero-Escribano, P. Malacrida, H. M. Hansen, U. Vej-Hansen, A. Velazquez-Palenzuela, V. Tripkovic, J. Schiøtz, J. Rossmeisl, I. E. L. Stephens, I. Chorkendorff, *Science (80).* **2016**, *352*, 73–76.
[171] L. Li, F. Abild-Pedersen, J. Greeley, J. K. Nørskov, *J. Phys. Chem. Lett.* **2015**, *6*, 3797–3801.
[172] S. De Waele, K. Lejaeghere, M. Sluydts, S. Cottenier, *Phys. Rev. B* **2016**, *235418*, 1–13.
[173] X. Liu, L. Sun, W. Q. Deng, *J. Phys. Chem. C* **2018**, *122*, 8306–8314.
[174] X. Zhang, J. X. Liu, B. Zijlstra, I. A. W. Filot, Z. Zhou, S. Sun, E. J. M. Hensen, *Nano Energy* **2018**, *43*, 200–209.
[175] J. Yu, X. Lin, J. Wang, J. Chen, W. Huang, *Appl. Surf. Sci.* **2009**, *255*, 9032–9039.
[176] P. Błon , A. Kiejna, Surf.Sci. **2007**, *601*, 123–133.
[177] L. Visto, H. L. Ruban, H. L. Skriver, J. Kollár, *Surf. Sci.* **1998**, *411*, 186–202.
[178] J. Lee, M. P. J. Punkkinen, S. Schönecker, Z. Nabi, K. Kádas, V. Zólyomi, Y. M. Koo, Surf.Sci.**2018**, *674*, 51–68.
[179] Y. Wen, J. Zhang, Solid.State.Commun.**2007**, *144*, 163–167.
[180] A. Patra, J. E. Bates, J. Sun, J. P. Perdew, Prc.Natl. Acad.Sci.USA. **2017**, 1–9.
[181] J. Wang, S. Wang, *Surf. Sci.* **2014**, *630*, 216–224.
[182] H. Wang, X. Nie, X. Guo, C. Song, *J. CO_2 Util.* **2016**, *15*, 107–114.
[183] U. Burghaus, *Prog. Surf. Sci.* **2014**, *89*, 161–217.
[184] G. C. Wang, L. Jiang, Y. Morikawa, J. Nakamura, Z. S. Cai, Y. M. Pan, X. Z. Zhao, *Surf. Sci.* **2004**, *570*, 205–217.
[185] F. Muttaqien, Y. Hamamoto, I. Hamada, K. Inagaki, Y. Shiozawa, K. Mukai, T. Koitaya, S. Yoshimoto, J. Yoshinobu, Y. Morikawa, *J. Chem. Phys.* **2017**, *147*, 094702.
[186] K. Czelej, K. Cwieka, K. J. Kurzydlowski, *Catal. Commun.* **2016**, *80*, 33–38.
[187] K. Duanmu, D. G. Truhlar, *J. Chem. Theory Comput.* **2017**, *13*, 835–842.
[188] B. Hammer, L. B. Hansen, J. K. Nørskov, *Phys. Rev. B - Condens. Matter Mater. Phys.* **1999**, *59*, 7413–7421.
[189] J. Wellendorff, K. T. Lundgaard, A. Møgelhøj, V. Petzold, D. D. Landis, J. K. Nørskov, T. Bligaard, K. W. Jacobsen, *Phys. Rev. B - Condens. Matter Mater. Phys.* **2012**, *85*, 32–34.
[190] J. Wellendorff, T. L. Silbaugh, D. Garcia-Pintos, J. K. Nørskov, T. Bligaard, F. Studt, C. T. Campbell, *Surf. Sci.* **2015**, *640*, 36–44.
[191] P. S. Schmidt, K. S. Thygesen, *J. Phys. Chem. C* **2018**, *122*, 4381–4390.
[192] F. Studt, F. Abild-Pedersen, J. B. Varley, J. K. Nørskov, *Catal. Letters* **2013**, *143*, 71–73.
[193] S. Mallikarjun Sharada, T. Bligaard, A. C. Luntz, G. J. Kroes, J. K. Nørskov, *J. Phys. Chem. C* **2017**, *121*, 19807–19815.
[194] H. Wang, X. Nie, Y. Chen, X. Guo, C. Song, *J. CO2 Util.* **2018**, *26*, 160–170.
[195] C. Liu, T. R. Cundari, A. K. Wilson, **2012**.
[196] S. Liu, Y. W. Li, J. Wang, H. Jiao, *J. Phys. Chem. C* **2015**, *119*, 28377–28388.
[197] H. L. Chen, H. T. Chen, J. J. Ho, *Langmuir* **2010**, *26*, 775–781.
[198] H. J. Li, J. J. Ho, *J. Phys. Chem. C* **2010**, *114*, 1194–1200.
[199] J. Ren, H. Guo, J. Yang, Z. Qin, J. Lin, Z. Li, *Appl. Surf. Sci.* **2015**, *351*, 504–516.
[200] P. Bothra, G. Periyasamy, S. K. Pati, *Phys. Chem. Chem. Phys.* **2013**, *15*, 5701–5706.
[201] K. Czelej, K. Cwieka, T. Wejrzanowski, P. Spiewak, K. J. Kurzydlowski, *Catal. Commun.* **2016**, *74*, 65–70.
[202] A. L. Maulana, R. I. D. Putra, A. G. Saputro, M. K. Agusta, Nugraha, H. K. Dipojono, *Phys. Chem. Chem. Phys.* **2019**, *21*, 20276–20286.
[203] K. Czelej, K. Cwieka, T. Wejrzanowski, P. Spiewak, K. J. Kurzydlowski, *Catal. Commun.* **2016**, *74*, 65–70.
[204] Y. F. Zhao, Y. Yang, C. Mims, C. H. F. Peden, J. Li, D. Mei, *J. Catal.* **2011**, *281*, 199–211.
[205] Y. Yang, J. Evans, J. A. Rodriguez, M. G. White, P. Liu, *Phys. Chem. Chem. Phys.* **2010**, *12*, 9909–9917.
[206] R. Van Den Berg, G. Prieto, G. Korpershoek, L. I. Van Der Wal, A. J. Van Bunningen, S. Lægsgaard-Jørgensen, P. E. De Jongh, K. P. De Jong, *Nat. Commun.* **2016**, *7*, DOI

10.1038/ncomms13057.
[207] M. Behrens, F. Studt, I. Kasatkin, S. Kühl, M. Hävecker, F. Abild-pedersen, S. Zander, F. Girgsdies, P. Kurr, B. Kniep, et al., *Science (80-.).* **2012**, *759*, 893–898.
[208] L. Liu, F. Fan, M. Bai, F. Xue, X. Ma, Z. Jiang, T. Fang, *Mol. Catal.* **2019**, *466*, 26–36.
[209] M. Zhang, Y. Wu, M. Dou, Y. Yu, *Catal. Letters* **2018**, *148*, 2935–2944.
[210] L. Liu, F. Fan, Z. Jiang, X. Gao, J. Wei, T. Fang, *J. Phys. Chem. C* **2017**, *121*, 26287–26299.
[211] M. Zhang, Y. Wu, M. Dou, Y. Yu, *Catal. Letters* **2018**, *148*, 2935–2944.
[212] X. Jiang, X. Nie, X. Wang, H. Wang, N. Koizumi, Y. Chen, X. Guo, C. Song, *J. Catal.* **2019**, *369*, 21–32.